

# Transition from time-variant to static networks: timescale separation in NIMFA SIS

Robin Persoons<sup>1,\*</sup>, Mattia Sensi<sup>2,3</sup>, Bastian Prasse<sup>4</sup>, Piet Van Mieghem<sup>1</sup>

<sup>1</sup>Faculty of Electrical Engineering, Mathematics and Computer Science, Delft University of Technology, P.O. Box 5031, 2600 GA Delft, The Netherlands. \*Corresponding author: [r.d.l.persoons@tudelft.nl](mailto:r.d.l.persoons@tudelft.nl)

<sup>2</sup>MathNeuro Team, Inria at Université Côte d’Azur, 2004 Rte des Lucioles, 06410 Biot, France

<sup>3</sup>Department of Mathematical Sciences “G. L. Lagrange”, Politecnico di Torino, Corso Duca degli Abruzzi 24, 10129 Torino Italy

<sup>4</sup>European Centre for Disease Prevention and Control (ECDC), Gustav III’s Boulevard 40, 169 73 Solna, Sweden.

May 23, 2023

## Abstract

We extend the N-intertwined mean-field approximation (NIMFA) for the Susceptible-Infectious-Susceptible (SIS) epidemiological process to time-varying networks. We investigate the timescale separation between disease spreading and topology updates of the network. We introduce the transition times  $\underline{T}(r)$  and  $\bar{T}(r)$  as the boundaries between the intermediate regime and the annealed (fast changing network) and quenched (static network) regimes, respectively. By analysing the convergence of static NIMFA processes, we analytically derive upper and lower bounds for  $\bar{T}(r)$ . We then illustrate these bounds numerically and we compare our simulations with a heuristic alternative for  $\bar{T}(r)$ . We show that, under our assumptions, the upper transition time  $\bar{T}(r)$  is almost entirely determined by the basic reproduction number  $R_0$ . The value of the upper transition time  $\bar{T}(r)$  around the epidemic threshold is large, which agrees with the current understanding that some real-world epidemics cannot be approximated with the aforementioned timescale separation.

**Keywords** Epidemic models · SIS process · NIMFA differential equations · Temporal networks · Timescale separation

**Mathematics Subject Classification** 92D30 · 92D25 · 34A34

**Disclaimer** The views and opinions expressed herein are the authors’ own and do not necessarily state or reflect those of ECDC. ECDC is not responsible for the data and information collation and analysis and cannot be held liable for conclusions or opinions drawn.

**Acknowledgements** This research has been funded by the European Research Council (ERC) under the European Union’s Horizon 2020 research and innovation programme (grant agreement No

101019718). MS was supported by the Italian Ministry for University and Research (MUR) through the PRIN 2020 project “Integrated Mathematical Approaches to Socio-Epidemiological Dynamics” (No. 2020JLWP23).

**Declarations** The authors have no competing interests to declare.

**Data Availability** Data sharing is not applicable to this article as no datasets were generated or analysed during the current study.

## 1 Introduction

The modelling of infectious disease spreading has been central in mathematical biology for almost a century (Anderson and May, 1991). Proper models of disease spreading are fundamental in describing, forecasting and controlling the evolution of epidemics. One of the most common assumptions is *homogeneous mixing*, which implies that any individual in the population is equally likely to encounter (and infect or get infected by) any other individual. Although homogeneous mixing greatly simplifies the analysis of the models, it is rather unrealistic, because individuals in real populations have more contacts with, for example, their family, friends and colleagues, which suggests contacts are heterogeneous. Such heterogeneous scenarios can be modelled as networks, in which nodes represent individuals and links represent contacts.

A vast majority of papers on epidemics in networks focuses on *static* networks (Mei et al., 2017; Nowzari et al., 2016; Pastor-Satorras et al., 2015). However, real-world contact networks are evolving, as individuals move frequently and encounter different groups (family, colleagues, commuters on public transport, etc.). In particular, contact networks evolve during an epidemic as well and changes in the contact network play a crucial role on the spread of epidemics (Holme, 2015; Holme and Saramäki, 2012).

The analysis of epidemics on time-variant networks is often under the assumption of timescale separation: either the network changes significantly faster than the spread of the disease or the epidemic evolves significantly faster than the topology updates of the network. Timescale separation of the network and the epidemic results in three regimes (Fig. 1). The three regimes correspond to the network topology updates being much faster (annealed regime), comparable (intermediate regime) or much slower (quenched regime) than the spread of the disease.

In the *quenched* regime, the network changes very slowly compared to the evolution of the epidemic. Quenched processes are well approximated with processes on static networks and therefore well studied over the last two decades. Indeed, as we will show in Section 1.3, the quenched regime assumes that, before each topology update, the epidemic has almost reached its equilibrium.

In the *annealed* regime, the epidemic evolves very slowly compared to the network. The epidemic spreads as on an “average” network. General results for the annealed regime show that the annealed process shares attributes with the static process on the edge-average graph (Kohar and Sinha, 2013; Valdano et al., 2018; Zhang et al., 2017). Additional results in the annealed regime have been derived under the degree-based mean-field theory by Pastor-Satorras and Vespignani (Devriendt and



**Fig. 1** Illustration of the timescale separation. The time between network topology updates  $\Delta t$  is increasing on the  $x$ -axis. The transition times  $\underline{T}(r)$  and  $\overline{T}(r)$  create the borders of the annealed and quenched regimes by including processes that are approximately annealed or quenched to the respective regimes, based on the accuracy tolerance  $r$ . The annealed regime is bounded from below by  $\Delta t = 0$ . The intermediate regime lies between the transition times  $\underline{T}(r)$  and  $\overline{T}(r)$ . The quenched regime extends from  $\Delta t = \overline{T}(r)$  to infinity.

Van Mieghem, 2017; Li et al., 2012; Pastor-Satorras and Vespignani, 2001a,b; Schwarzkopf et al., 2010).

The *intermediate* regime, that resides between the quenched and annealed regimes, is difficult to analyse. However, it is considered to be the most important in real world scenarios (Holme, 2015; Holme and Liljeros, 2014; Leitch et al., 2019; Perra et al., 2012; Stehlé et al., 2011). Diseases spread at a timescale comparable to the timescale of the movement of individuals.

In this work, we introduce the lower and upper transition times  $\underline{T}(r)$  and  $\overline{T}(r)$  as the boundaries between the three timescale regimes in Fig. 1. In particular, we provide analytical bounds on the upper transition time  $\overline{T}(r)$ , which indicates whether the contact network can be considered approximately static. As a function of the accuracy tolerance  $r$  these transition times indicate to which regime a process with a specific time between topology updates (inter-update time)  $\Delta t$  belongs. The dependence on an accuracy tolerance  $r$  is required, because the annealed regime for small inter-update times  $\Delta t$  and the quenched regime for large inter-update times  $\Delta t$  only describe the exact behaviour for  $\Delta t \rightarrow 0$  and  $\Delta t \rightarrow \infty$ , respectively. Indeed, only approximately quenched and approximately annealed processes exist outside of these limits. We introduce the accuracy tolerance  $r$  to extend the quenched and annealed regimes to include, per definition, these approximately quenched and annealed processes. When the error due to the quenched or annealed approximation does not exceed the accuracy tolerance  $r$ , the process is considered quenched or annealed. These transition times are the boundaries of the intermediate regime (Fig. 1), when an error due to timescale separation of at most  $r$  is allowed.

Epidemics on time-varying networks are studied analytically in (Leitch et al., 2019; Ogura and Preciado, 2016; Paré et al., 2015, 2017a,b; Perra et al., 2012; Schwarzkopf et al., 2010) and results based on simulations and analysis of real-world data are found in (Guo et al., 2021; Han et al., 2023; Kotnis and Kuri, 2013; Lieberman et al., 2005; Nadini et al., 2018; Prakash et al., 2010; Ren and Wang, 2014; Stehlé et al., 2011; Vestergaard and Génois, 2015). However, to the best of the authors' knowledge, our quantification of the boundaries in Fig. 1 is novel.

The paper is structured as follows. First, we briefly recall the N-Intertwined Mean Field Approximation (NIMFA) SIS process (Van Mieghem et al., 2009) in Section 1.1. In Section 1.2, we present our extension of the NIMFA model to time-varying networks. In Section 1.3, we discuss the timescale regimes and timescale separation in more depth. In Section 2, we formally introduce the upper transi-

tion time  $\bar{T}(r)$  and show numerical results on the upper transition time  $\bar{T}(r)$ . In Section 3, we derive upper and lower bounds on the upper transition time  $\bar{T}(r)$  and numerically compare them with results from Section 2. We conclude in Section 4.

### 1.1 The Markovian and NIMFA SIS processes

We consider the homogeneous continuous-time Markovian SIS process on a static network, represented by a simple undirected contact graph  $G(N, L)$ , with corresponding  $N \times N$  symmetric adjacency matrix  $A$ , where  $a_{ij} = 1$  if nodes  $i$  and  $j$  are connected and  $a_{ij} = 0$  otherwise (Van Mieghem, 2011a). A simple graph has no self-loops and thus  $a_{ii} = 0$  for all nodes  $i$ . These requirements on the adjacency matrix hold for all graphs considered in this paper.<sup>1</sup>

The Markovian SIS process has states specified by Bernoulli random variables  $X_i \in \{0, 1\}$  for each node  $i$ . If  $X_i = 1$  the node  $i$  is *infected*, else the node  $i$  is *healthy* but *susceptible*. At a time  $t$ , the node  $i$  is infected with probability  $v_i(t) = \Pr[X_i(t) = 1]$  and healthy with probability  $1 - v_i(t)$ . We assume that the infection attempts from an infected node  $i$  to a healthy node  $j$  are Poisson processes with infection rates  $\beta$ . Each node also has a Poisson curing process with curing rate  $\delta$ . The effective infection rate is defined as  $\tau = \frac{\beta}{\delta}$ . The vector of all  $v_i(t)$  is denoted as  $V(t) = [v_1(t) \ v_2(t) \ \dots \ v_N(t)]^T$ . We define the *prevalence*  $y(t)$ , which is the average fraction of infected nodes:

$$y(t) = \frac{1}{N} \sum_{i=1}^N v_i(t). \quad (1)$$

The SIS model exhibits a *phase transition* at the epidemic threshold  $\tau_c$ . If  $\tau < \tau_c$ , the epidemic dies out exponentially fast (Ganesh et al., 2005). If  $\tau > \tau_c$ , the epidemic lasts very long<sup>2</sup> (Van Mieghem, 2013). For any effective infection rate  $\tau$  the epidemic will eventually die out (Van Mieghem, 2020), since the overall healthy state  $V(t) = 0$  is the only steady state of the Markovian SIS process. The fact that the Markov state  $X_i(t)$  is a Bernoulli random variable, for which  $\mathbb{E}[X_i] = \Pr[X_i = 1]$  holds, leads to a differential equation for the infection probability of node  $i$ , first proposed in (Cator and Van Mieghem, 2012):

$$\frac{d\mathbb{E}[X_i]}{dt} = \mathbb{E} \left[ -\delta X_i + \beta(1 - X_i) \sum_{j=1}^N a_{ij} X_j \right] = -\delta \mathbb{E}[X_i] + \beta \sum_{j=1}^N a_{ij} \mathbb{E}[X_j] - \beta \sum_{j=1}^N a_{ij} \mathbb{E}[X_i X_j]. \quad (2)$$

The joint probability  $\mathbb{E}[X_i X_j] = \Pr[X_i = 1, X_j = 1]$  is remarkably complicated (Cator and Van Mieghem, 2012; Van Mieghem, 2014). Therefore, we confine our analysis to the N-Intertwined Mean Field Approximation (NIMFA) (Van Mieghem, 2011b; Van Mieghem et al., 2009) for the SIS model. NIMFA replaces in the Markovian SIS process the random variable  $X_i$  with the expectation  $\mathbb{E}[X_i]$  and  $\mathbb{E}[X_i X_j]$  reduces to  $\mathbb{E}[X_i] \mathbb{E}[X_j]$ . Then, the mean-field approximation the governing NIMFA equations for a static network are given by the differential equations (Lajmanovich and Yorke, 1976)

$$\frac{dv_i(t)}{dt} = -\delta v_i(t) + \beta(1 - v_i(t)) \sum_{j=1}^N a_{ij} v_j(t), \quad i = 1, 2, \dots, N. \quad (3)$$

<sup>1</sup>We will write “For any/Given a graph  $G$ ,” instead of “For any/Given a graph  $G$ , with adjacency matrix  $A$  obeying  $a_{ij} = a_{ji}$  and  $a_{ii} = 0$  for all nodes  $i$  and  $j$ ,” for clarity.

<sup>2</sup>Technically, there is a non-zero probability that the epidemic dies out fast for  $\tau > \tau_c$  in the Markovian SIS model, since the probability of curing before infecting anyone is non-zero for any  $\tau$ .

The phase transition occurs in NIMFA SIS at the first-order NIMFA epidemic threshold  $\tau_c^{(1)} = \frac{1}{\lambda_1(A)}$ , where  $\lambda_1(A)$  is the largest eigenvalue of the adjacency matrix  $A$ . Additionally, the NIMFA epidemic threshold lower bounds the Markovian SIS epidemic threshold  $\tau_c^{(1)} < \tau_c$  for all networks<sup>3</sup>. The NIMFA steady-state prevalence is denoted as  $y_\infty$  and the infection probability of node  $i$  in the steady state is denoted as  $v_{\infty,i}$ . NIMFA has a non-trivial steady state ( $y_\infty \neq 0$ ) for  $\tau > \tau_c^{(1)}$ , which corresponds to the metastable state in the Markovian SIS process. Therefore, analysis of the NIMFA steady state allows insights into the metastable state of the Markovian SIS process. When  $V(0) \neq 0$  and  $V(0) \neq V_\infty = [v_{\infty,1}(t) \ v_{\infty,2}(t) \ \dots \ v_{\infty,N}(t)]^T$ , the NIMFA process will tend (Khanafar et al., 2016; Lajmanovich and Yorke, 1976), for  $t \rightarrow \infty$ , to either the steady state  $V_\infty = 0$  (if  $\tau \leq \tau_c^{(1)}$ ) or to an upper bound for the Markovian SIS metastable state  $V_\infty > 0$  (if  $\tau > \tau_c^{(1)}$ ). Strictly speaking, the origin  $V(t) = 0$  is also a steady state for  $\tau > \tau_c^{(1)}$ . However, if  $\tau > \tau_c^{(1)}$ , then we only denote the non-negative vector  $V_\infty > 0$  as the steady state.

## 1.2 NIMFA on time-variant networks

The topology of a time-variant network is represented at time  $t$  by a simple undirected contact graph  $G(t) = G(N, L(t))$ . At all times  $t$ , the network has the same  $N$  nodes, but the amount of links  $L(t)$  may vary. The contact graph  $G(t)$  is represented by its  $N \times N$  symmetric adjacency matrix  $A(t)$ .

We denote with  $t_m$  the occurrence time of the  $m$ -th topology change. Within the interval  $[t_{m-1}, t_m)$ , with length  $T_m = t_m - t_{m-1}$ , the network remains static. We denote the graph  $G(t)$  during the interval  $t_{m-1} \leq t < t_m$  by  $G_m$  and similarly the adjacency matrix  $A(t) = A_m$  for  $t_{m-1} \leq t < t_m$ , with elements  $a_{ij}(t) = (a_m)_{ij}$ . Denoting the total amount of topologies by  $M$ , the complete interval  $[t_0, t_M]$  has exactly  $M - 1$  topology updates and the sequences of graphs and adjacency matrices are denoted by:

$$\mathcal{G} := \{G_1, \dots, G_M\}, \quad \mathcal{A} := \{A_1, \dots, A_M\}.$$

We will call the times  $\{t_0, \dots, t_M\}$  the *update times* and the lengths of the intervals  $[t_{m-1}, t_m)$ , namely the set  $\{T_1, \dots, T_M\}$ , the *inter-update times*. In a time-variant network, the NIMFA epidemic threshold equals  $\tau_c^{(1)}(G_m) = \frac{1}{\lambda_1(A_m)}$ , which varies with the topology  $m$ . For each graph  $G_m$  or adjacency matrix  $A_m$  and for a fixed effective infection rate  $\tau$ , we define the basic reproduction number

$$(R_0)_m = R_0(G_m, \tau) := \frac{\tau}{\tau_c^{(1)}(G_m)} = \frac{\beta}{\delta} \lambda_1(A_m). \quad (4)$$

The phase transition coincides with  $R_0 = 1$ , which is equivalent to an effective infection rate  $\tau = \tau_c^{(1)}$ . We say that  $R_0(t) = (R_0)_m$  if  $t_{m-1} \leq t < t_m$ . The governing NIMFA equations for the entire time period  $[t_0, t_M]$  for a node  $i$  are given by:

$$\left\{ \begin{array}{l} \frac{dv_i(t)}{dt} = -\delta v_i(t) + \beta(1 - v_i(t)) \sum_{j=1}^N (a_1)_{ij} v_j(t), \quad t \in [t_0, t_1), \\ \vdots \\ \frac{dv_i(t)}{dt} = -\delta v_i(t) + \beta(1 - v_i(t)) \sum_{j=1}^N (a_M)_{ij} v_j(t), \quad t \in [t_{M-1}, t_M). \end{array} \right. \quad (5)$$

<sup>3</sup>NIMFA upper bounds the infection probability in the Markovian SIS process (Van Mieghem et al., 2009). Specifically, when  $\tau_c > \tau > \tau_c^{(1)}$  NIMFA will not die out, but a Markovian SIS process will die out fast.

Recalling the definition of the vector  $V(t) := [v_1(t) v_2(t) \dots v_N(t)]^T$ , the matrix representation of (5) on each interval  $[t_{m-1}, t_m)$  is

$$\frac{dV(t)}{dt} = (\beta A_m - \delta I)V(t) - \beta \text{diag}(V(t))A_m V(t), \quad (6)$$

where  $I$  denotes the  $N \times N$  identity matrix and  $\text{diag}(x)$  is the diagonal matrix with the elements  $x_i$  of the  $N \times 1$  vector  $x$  on the diagonal. Since the derivative of  $v_i(t)$  exists on the entire interval  $[t_0, t_M)$ , we know that  $v_i(t)$  is continuous on  $[t_0, t_M)$ . The starting conditions at each update time  $v_i(t_m)$  are the limits  $v_i(t_m - \varepsilon)$  as  $\varepsilon \rightarrow 0^+$ . It follows from (5) that the derivative is, in general, discontinuous at  $t_m$ :

$$\left. \frac{dv_i}{dt} \right|_{t=t_m-\varepsilon} \neq \left. \frac{dv_i}{dt} \right|_{t=t_m},$$

in the limit  $\varepsilon \rightarrow 0^+$  if  $A_m \neq A_{m+1}$ .

We will, without loss of generality, take  $\delta = 1$ , because for any  $\delta > 0$ , we can rescale the time variable in units of the average curing time  $\frac{1}{\delta}$ . Indeed, we replace the time  $t$  with  $\theta = \delta t$  in (3), while keeping the rates the same in the new time units:

$$\frac{dv_i}{d\theta} = -v_i(\theta) + \tau(1 - v_i(\theta)) \sum_{j=1}^N a_{ij} v_j(\theta), \quad (7)$$

which are the “rescaled” NIMFA governing equations. The same method can be applied to the system (5), where an equivalent system with  $\delta = 1$  is found. The intervals  $[t_{m-1}, t_m)$  of the “rescaled” system are measured in units of the average curing time  $\frac{1}{\delta}$ . In the following, because we will use (7) instead of (3), we write  $t$  instead of  $\theta$  when using (7) for clarity.

### 1.3 Timescale separation and the transition times

In this section, we explore the interplay between the timescale of the epidemic process and the timescale of the topology updating process. We assume here that the inter-update times  $T_m$  are constant and equal to  $\Delta t$ . The timescales of the epidemic process are characterized by the average infection time  $\frac{1}{\beta}$  between infection attempts on links and the average curing time  $\frac{1}{\delta}$ . Fig. 2 shows temporal NIMFA processes that correspond to the three regimes in Fig. 1. Three processes with the same infection rate  $\beta$ , the same curing rate  $\delta$  and random contact graphs  $G_m$  with the same distribution, but with different inter-update times  $\Delta t$  are illustrated. The red line in Fig. 2 shows the averaging behavior of the annealed regime. The blue line illustrates the convergence to equilibrium on each network topology of the quenched regime. The black line shows an irregular process, which corresponds to the intermediate regime.

We introduce the transition times  $\underline{T}(r)$  and  $\overline{T}(r)$  as functions of the sequence of graphs  $\mathcal{G}$ , the infection rate  $\beta$ , the curing rate  $\delta$  and the accuracy tolerance  $r$ . The transition times or the boundaries of the regimes  $\underline{T}(r)$  and  $\overline{T}(r)$  are only meaningful as a function of the accuracy tolerance  $r$ . The accuracy tolerance  $r$  identifies temporal processes that can be approximated well with quenched or annealed processes. Here, the accuracy tolerance  $r$  can be lowered to increase the accuracy of the approximation. In this work, we restrict ourselves to an analysis of the upper transition time  $\overline{T}(r)$ .

When  $\Delta t$  tends to  $\infty$ , the temporal process gains a form of the Markov property, where the graphs  $\{G_k\}_{k < m}$  have a decreasing influence on the state of the process at time  $t = t_m$ , when  $\Delta t$  increases.

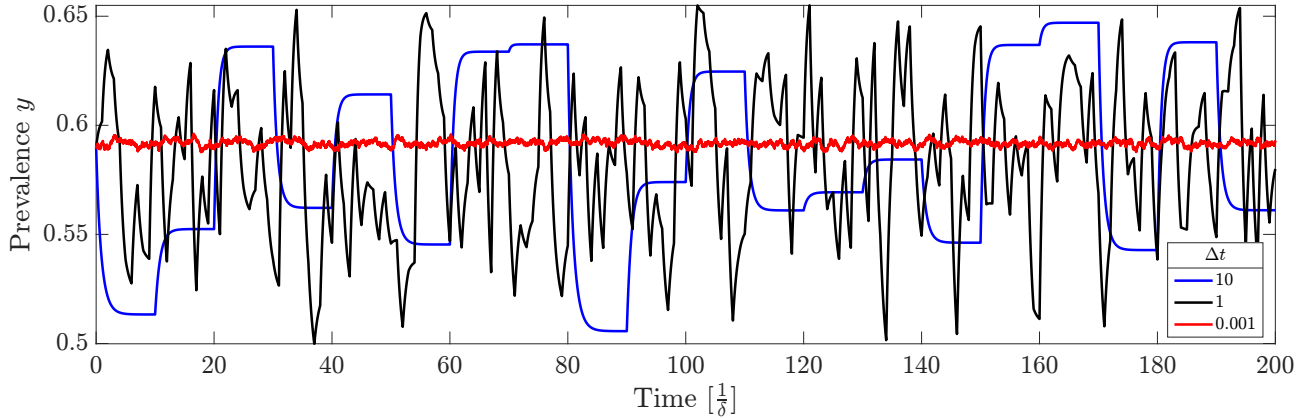


**Fig. 2** time-variant NIMFA SIS for different inter-update times  $\Delta t$ . Parameters: graph size  $N = 50$ ; infection rate  $\beta = 0.1$ ; curing rate  $\delta = 1$ . Every graph is an ER random graph, where the link density  $p$  is picked uniformly at random from the interval  $[0.4, 0.6]$ . The red line (small inter-update time  $\Delta t = 0.001$ ) shows the averaging behavior when nearing the annealed regime. The black line (medium inter-update time  $\Delta t = 1$ ) shows the unpredictability of the intermediate regime. The blue line (large inter-update time  $\Delta t = 10$ ) shows the converging on each topology from the quenched regime.

The Markov property arises from the fact that, in the quenched limit of  $\Delta t \rightarrow \infty$ , the static NIMFA SIS process will tend to its steady-state vector  $V_\infty$  from any starting point  $V(0) \neq 0$ . Therefore, when  $\Delta t$  increases, the difference between the prevalence  $y(t_m)$  at the end of the interval  $[t_{m-1}, t_m)$  and the steady-state prevalence  $y_\infty$  decreases independent of  $y(t_{m-1})$ , when  $y(t_{m-1}) \neq 0$ .

The complete intervals  $[t_{m-1}, t_m)$  possesses a similar Markov property, since the starting state  $V(t_{m-1})$  and the graph  $G_m$  completely determine  $V(t)$  for  $t \in [t_{m-1}, t_m)$ . Recalling that, when  $\Delta t$  tends to  $\infty$ ,  $V(t_{m-1})$  is determined only by the graph  $G_{m-1}$ , the interval  $[t_{m-1}, t_m)$  is then fully determined by the graphs  $G_{m-1}$  and  $G_m$ . When  $(R_0)_m > 1$ , the steady-state vector  $V_\infty(G_m)$  approximates the infection probability vector  $V(t)$  at the end of the  $m$ -th interval  $V(t_m)$ . The case of  $R_0(G_{m-1}) \leq 1$  should be treated carefully, because the steady state  $V_\infty = 0$  describes an epidemic which is completely extinct. Hence, when  $R_0(G_{m-1}) < 1$  in the quenched regime, we should approximate the entries of the infection probability vector at the topology update as  $V_i(t_{m-1}) \geq \epsilon$ , with a small  $0 < \epsilon \ll 1$ , because in NIMFA  $V(t) = 0$  is only actually reached in the limit as  $t \rightarrow \infty$  and would mean that the epidemic process stops.

These Markov-like attributes are what we use to can quantify a process as “quenched”. We investigate whether we can specify the inter-update time  $\Delta t = \bar{T}(r)$ , as a function of the effective infection rate  $\tau$ , the sequence of graphs  $\mathcal{G}$  and an accuracy tolerance  $r$ , such that for  $\Delta t \geq \bar{T}(r)$ , the NIMFA SIS process will reach the steady-state prevalence  $y_\infty$  on each interval  $[t_{m-1}, t_m)$  with an error  $|y_\infty - y(t_m)| \leq r$ , i.e. at most the accuracy tolerance  $r$ .

In order to define a well-posed problem, we will make the following simplifying assumptions:

1. The number of nodes  $N$  and the number of topologies  $M$  are fixed and finite.
2. The inter-update times  $T_m = t_m - t_{m-1}$  are constant and equal to  $T_m = \Delta t$ .

3. We consider the mean-field NIMFA SIS process instead of the Markovian SIS process.
4. We confine ourselves to homogeneous SIS with link infection rates  $\beta_{ij} = \beta$  for all links  $i \sim j$  and nodal curing rates  $\delta_i = \delta$  for all nodes  $i$ .
5. In our numerical analysis all graphs  $G_m$  are Erdős-Rényi graphs<sup>4</sup>  $G(N, p)$ , where the link density  $p$  is a uniformly distributed random variable. In Appendix A concerns whether ER-graphs are representative of general graphs are addressed.
6. In simulations we assume values of  $N = 50$  and  $\beta = 0.1$ . Taking larger values of  $N$  leads to two problems: 1) ER-graphs becoming incredibly regular; and 2) running times become too large. Increasing  $\beta$  leads to the problem that when  $\tau \geq \tau_c^{(1)}(G)$  for a disconnected graph  $G$ , the basic reproduction number no longer corresponds to the slowest converging component. Working around this issue would again increase running times too much. Decreasing  $\beta$  quickly reduces all graphs below the epidemic threshold.

## 2 The upper transition time

An intuitive first definition of the upper transition time  $\bar{T}(r)$  for a fixed effective infection time  $\tau$ , is the smallest time  $t$  such that the error  $|y(t) - y_\infty| \leq r$  for all graphs  $G_m \in \mathcal{G}$  and all starting values  $v_i(0) \in (0, 1]$  for all nodes  $i$ . This definition implies that the steady state is reached up to the accuracy tolerance  $r$  on each contact graph  $G_m$ . However, for small starting infection probability vectors  $\|V(0)\|_1 = \varepsilon \ll 1$  and graphs  $G$  with basic reproduction number  $R_0(G, \tau) > 1$ , the time of convergence to reach  $|y(t) - y_\infty| \leq r$  can be made arbitrarily long by selecting a sufficiently small  $\varepsilon$ , as proved in the following Lemma.

**Lemma 1.** *Given a graph  $G$ , an effective infection rate  $\tau > \tau_c^{(1)}$ , an arbitrary large time  $\mathcal{T}$  and an accuracy tolerance  $r < y_\infty$ , there exists a starting infection probability vector  $V(0) = \varepsilon(r)u > 0$ , where  $u$  is the all-one vector, such that  $|y(t) - y_\infty| > r$  for all  $t \leq \mathcal{T}$ .*

**Proof.** We consider the starting infection probability vector  $V(0) = \varepsilon(r)u$ . We will upper bound the prevalence  $y(t)$  and then substitute the starting condition and show that  $|y(\mathcal{T}) - y_\infty| > r$ . The derivative  $\frac{dy(t)}{dt}$  of the prevalence  $y(t)$  in (1) follows from (7) as:

$$\frac{dy(t)}{dt} = -y(t) + \frac{\tau}{N} \sum_{i=1}^N (1 - v_i(t)) \sum_{j=1}^N a_{ij} v_j(t).$$

Since  $(1 - v_i(t)) \leq 1$  and  $a_{ij} \leq 1$ , we find that

$$\frac{dy(t)}{dt} < -y(t) + \frac{\tau}{N} \sum_{i=1}^N \sum_{j=1}^N v_j(t) = -y(t) + \tau N y(t),$$

where we have a strict inequality, because self-loops are non-existent in a contact graph ( $a_{ii} = 0$ ). Using Grönwall's inequality on the differential inequality  $\frac{dy(t)}{dt} < (\tau N - 1)y(t)$  gives us an upper

---

<sup>4</sup>An Erdős-Rényi random graph  $G_p(N)$  is characterized by the link between each pair of the  $N$  nodes existing with probability  $p$ , independent of any other link.

bound on the prevalence  $y(t)$ :

$$y(t) < y(0)e^{(\tau N-1)t}. \quad (8)$$

The starting infection probability vector  $V(0) = \varepsilon(r)u$ , implies that the starting prevalence  $y(0) = \varepsilon(r)$ . After picking  $\varepsilon(r) = \frac{y_\infty - r}{e^{(\tau N-1)\mathcal{T}}}$ , such that  $y(0) = \varepsilon(r) < y_\infty$ . The difference  $|y(t) - y_\infty|$  is:

$$|y(t) - y_\infty| = y_\infty - y(t) > y_\infty - (y_\infty - r) \frac{e^{(\tau N-1)t}}{e^{(\tau N-1)\mathcal{T}}}.$$

Since  $\frac{e^{(\tau N-1)t}}{e^{(\tau N-1)\mathcal{T}}} \leq 1$  for times  $t \leq \mathcal{T}$ , we find  $|y(t) - y_\infty| > y_\infty - y_\infty + r = r$ , which proves the Lemma.  $\square$

To ensure that the upper transition time  $\bar{T}(r)$  is finite, we bound the infection probabilities  $v_i(0) \geq r$ , with the accuracy tolerance  $r$  and define the upper transition time  $\bar{T}(r)$  for fixed effective infection rate  $\tau$  as

$$\bar{T}(r) = \min_{t \geq 0} \{ |y(t; G_m) - y_\infty(G_m)| \leq r ; \forall G_m \in \mathcal{G} \text{ and } \forall V(0) \text{ s.t. } v_i(0) \in [r, 1] ; \forall i = 1, \dots, N \}, \quad (9)$$

where  $y(t; G_m)$  indicates the NIMFA SIS prevalence on a fixed graph  $G_m$ . In static processes, the restriction  $v_i(0) \geq r$  for all nodes  $i$  guarantees that  $|y(\bar{T}(r)) - y_\infty| \leq r$  for any graph  $G$ . However, in a temporal process, given an accuracy tolerance  $r$ , we can select a sequence of graphs, such that  $y(t_{m(r)}) < r$  after the first  $m(r)$  intervals, dependent on the accuracy tolerance  $r$ , but independent of the starting infection probability vector  $V(0)$ . Then, for a graph  $G_{m+1}$  with basic reproduction number  $R_0 > 1$  on the next interval  $[t_{m(r)}, t_{m(r)+1})$ , it can happen that  $|y(t_{m+1}) - y_\infty| > r$ . Therefore, if the prevalence  $y(t)$  of the temporal process decreases below  $r$ , the prevalence at each following graph update  $y(t_m) \big|_{t_m > t}$  is no longer guaranteed to be within the accuracy tolerance  $r$  around the steady-state prevalence  $y_\infty$  when  $\Delta t \geq \bar{T}(r)$ . While it would be preferable that  $\Delta t \geq \bar{T}(r)$  implies  $|y(t_m) - y_\infty| \leq r$  for all topologies  $m$  and all starting infection probability vectors  $V(0)$ , Lemma 1 shows that a lower bound on the starting infection probabilities  $v_i(0)$  is necessary for the upper transition time  $\bar{T}(r)$  to be finite.

## 2.1 Numerical results

The upper transition time  $\bar{T}(r)$  can only be determined approximately, since there is no closed formula for the steady-state prevalence  $y_\infty$  for general graphs. Therefore, we numerically approximate  $y_\infty$  with the prevalence  $y(t_{\max})$ , for some large simulation time  $t_{\max}$ . Alternatively, one can solve the NIMFA equations (7) numerically to calculate the steady state prevalence  $y_\infty$ . However, because of the bifurcation of the steady-state it can be hard to guarantee that the numerical solver does not find the all-healthy state  $V = 0$  when looking for a small steady-state vector  $0 < V_\infty \ll 1$ .

Fig. 3 shows the numerical approximation of the upper transition time  $\bar{T}(r)$ , with accuracy tolerance  $r = 10^{-4}$ , for different values of the basic reproduction number  $R_0$  and the starting prevalence  $y(0)$ . Specifically, the starting values are  $V(0) = y(0)u$  for different values of  $y(0)$ . As mentioned above, the steady-state prevalence  $y_\infty$  is approximated with as  $y_\infty \approx y(10^4)$ , by taking  $t_{\max} = 10^4$ . The sharp lines in Fig. 3 show that the upper transition time  $\bar{T}(r)$  is almost fully determined for each graph by the basic reproduction number  $R_0$ . Additionally, Fig. 3 illustrates the asymptotic behavior around

$R_0 = 1$ . In particular, Fig. 3 shows that the upper transition time  $\bar{T}(r)$  is zero for  $y(0) = 10^{-4}$  (blue line) if  $R_0 \leq 1$ . The inset in Fig. 3 shows dips below the curves if the starting value  $y(0)$  is approximately equal to the steady-state prevalence  $y_\infty$  for the corresponding values of the basic reproduction number  $R_0$ .

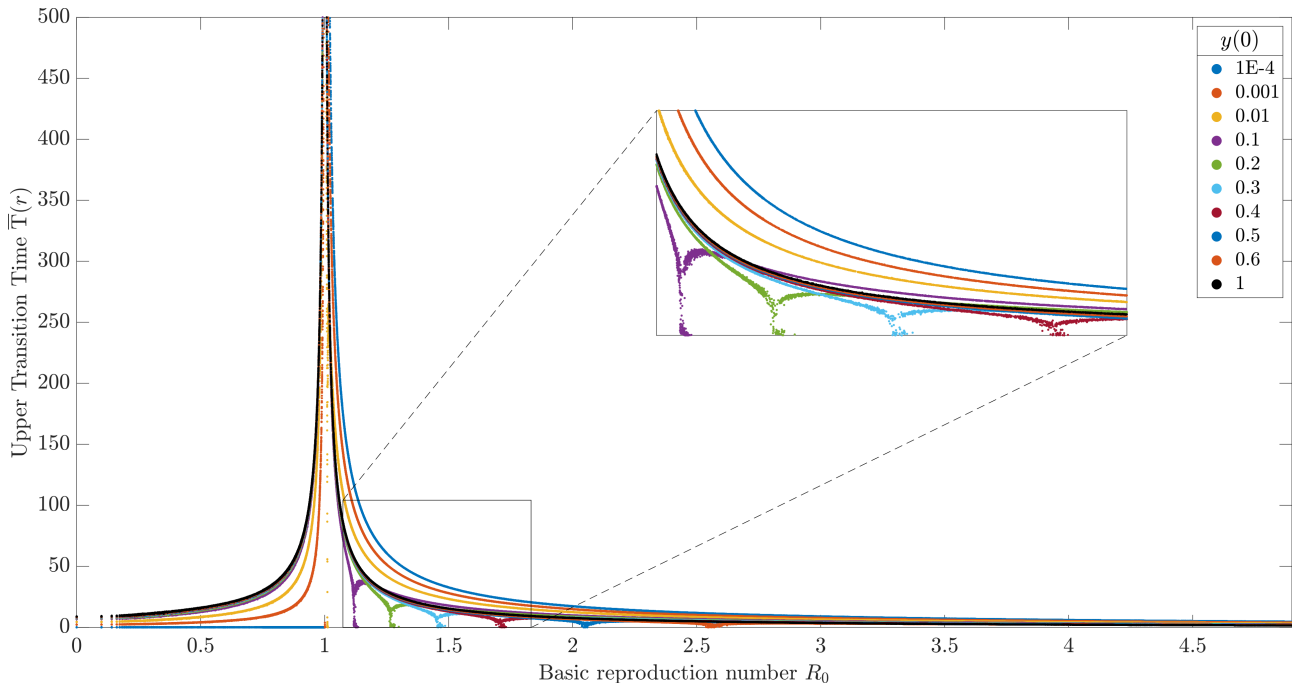


**Fig. 3** The upper transition time  $\bar{T}(r)$  versus the basic reproduction number  $R_0$  for different values of the starting prevalence  $y(0)$ . The chosen parameters are a graph size  $N = 50$ , accuracy tolerance  $r = 10^{-4}$ , infection rate  $\beta = 0.1$ . Each graph is an Erdős-Rényi graph  $G_p(N)$  with link density  $p$  chosen uniformly at random:  $p \sim \text{Unif}(0,1)$ . For  $R_0 > 1$ , the small values of  $y(0)$  correspond to the top curves, i.e. to a higher upper transition time  $\bar{T}(r)$ . For  $R_0 < 1$ , the small values of  $y(0)$  correspond to the bottom curves, i.e. to a lower upper transition time  $\bar{T}(r)$ . For  $y(0) = 10^{-4}$  the upper transition time  $\bar{T}(r)$  is zero per definition. To determine the upper transition time  $\bar{T}(r)$  we approximate the steady-state prevalence  $y_\infty$  with  $y_\infty \approx y(t_{\max}) = y(10^4)$ . The inset shows the dips below the curves in more detail.

## 2.2 Derivative Convergence time

As an heuristic for the upper transition time  $\bar{T}(r)$  we consider the derivative convergence time  $t^*$ , which does not depend on  $y_\infty$ . The derivative convergence time is defined as the first time  $t$  during a NIMFA SIS process obeying the inequality  $|v_i(t+h) - v_i(t)| \leq hr^*$  for all nodes  $i$  in the graph  $G$ :

$$t^* = \min_{t \geq 0} \{ |v_i(t+h) - v_i(t)| \leq hr^* ; \forall i = 1, \dots, N \}, \quad (10)$$

where  $h$  is a step-size parameter and  $r^*$  is an accuracy tolerance. We denote this accuracy tolerance as  $r^*$  instead of  $r$ , because the derivative convergence time  $t^*(r^*)$  does not scale in the same way with the accuracy tolerance  $r^*$  as the upper transition time  $\bar{T}(r)$  with the accuracy tolerance  $r$ .

The derivative convergence time  $t^*$  does not depend on the steady-state prevalence  $y_\infty$  and therefore does not need information about future times. The derivative convergence time can be determined without knowledge of the prevalence at future times. When approximating  $y_\infty$  with the prevalence  $y(t_{\max})$ , the simulation determining the derivative convergence can be stopped at the time  $t = t^*$  instead of the time  $t = t_{\max}$ . Then, numerically determining the derivative convergence time  $t^*$  requires significantly less time than determining the upper transition time  $\bar{T}(r)$ . When finding  $y_\infty$  by solving the NIMFA equations, the time saved is reduced, but determining the derivative convergence time  $t^*$  will potentially still be faster as the calculation of  $y_\infty$  can be skipped.

Fig. 4 shows the values of the derivative convergence time  $t^*$  for different values of the basic reproduction number  $R_0$  and the starting prevalence  $y(0)$ . Specifically, the starting values were  $V(0) = y(0)u$  for different values of  $y(0)$ . The inset in Fig. 4 shows sharp dips below the curves due to the starting value  $y(0)$  being close to  $y_\infty$  for that specific value of  $R_0$ , resulting in fast convergence. When the prevalence  $y(0)$  is small, the initial changes in the prevalence are also small, resulting in the process instantaneously reaching the stopping criterion  $|v_i(t+h) - v_i(t)| \leq hr^*$ . Fig. 4 illustrates a trend similar to the one shown in Fig. 3. Indeed, both the upper transition time  $\bar{T}(r)$  and the derivative convergence time  $t^*(r^*)$  show the same asymptotic behaviour around  $R_0 = 1$  and have the same dips when the starting prevalence  $y(0)$  is close to the steady-state prevalence  $y_\infty$ . Like the upper transition time  $\bar{T}(r)$ , the derivative convergence time  $t^*$  is almost fully determined for each graph by the basic reproduction number  $R_0$ . The differences are more clear in Fig. 5, in which the log-scale shows that the derivative convergence time  $t^*(r^*)$  has larger tails than the upper transition time  $\bar{T}(r)$ .

In order to upper bound the upper transition time  $\bar{T}(r)$  with the derivative convergence time  $t^*(r^*)$ , which would allow to save computation time, it is of interest to know which value of  $r^*$  is sufficient for some arbitrary value of  $r$  and sequence of graphs  $\mathcal{G}$ .

We compare the convergence criteria  $|y(t+h) - y(t)| < hr^*$  and  $|y(t) - y(t_{\max})| < r$  for  $t_{\max} = 10^4$  and different values of  $r$  and  $r^*$ . The resulting Fig. 5 shows that, when  $r$  decreases by a factor of 10,  $r^*$  has to decrease by a factor of  $10^2$  to remain an upper bound for all values of  $R_0$ . In Fig. 5, the lowest  $r^*$  for which the upper transition time  $\bar{T}(r)$  is upper bounded by the derivative convergence time  $t^*(r^*)$  is  $r^* = 10^{-2a}$  when  $r = 10^{-a}$ , for some  $a \in \mathbb{N}$ . Indeed, we have that the derivative convergence times  $t^*(r^*)$  with  $r^* = 10^{-2}, 10^{-4}, 10^{-6}, 10^{-8}$  bound the upper transition times  $\bar{T}(r)$  with  $r = 10^{-1}, 10^{-2}, 10^{-3}, 10^{-4}$  respectively.

### 3 Bounds for the upper transition time

We bound the convergence towards the steady state  $V_\infty$  from above and below separately. We write  $V(t) \geq V_\infty$  if  $v_i(t) \geq v_{\infty,i}$  for all nodes  $i$  and similarly,  $V(t) \leq V_\infty$  if  $v_i(t) \leq v_{\infty,i}$  for all nodes  $i$ . We call the convergence to the steady state from an infection probability vector  $V(t) \geq V_\infty$  the *decay* of  $V(t)$  and convergence to the steady state from an infection probability vector  $V(t) \leq V_\infty$  the *growth* of  $V(t)$ . We upper bound the upper transition time  $\bar{T}(r)$  by deriving bounds for decay (Section 3.1) and for growth (Section 3.2) and taking the maximum to combine them in Section 3.3. The following Theorem 1 (Theorem 5 in (Prasse et al., 2021)) tells us that the slowest allowed growth starts in  $V(0) = ru$  and the slowest decay starts in  $V(0) = u$  when the contact graph  $G$ , the curing rate  $\delta$  and the infection rate  $\beta$  are fixed.

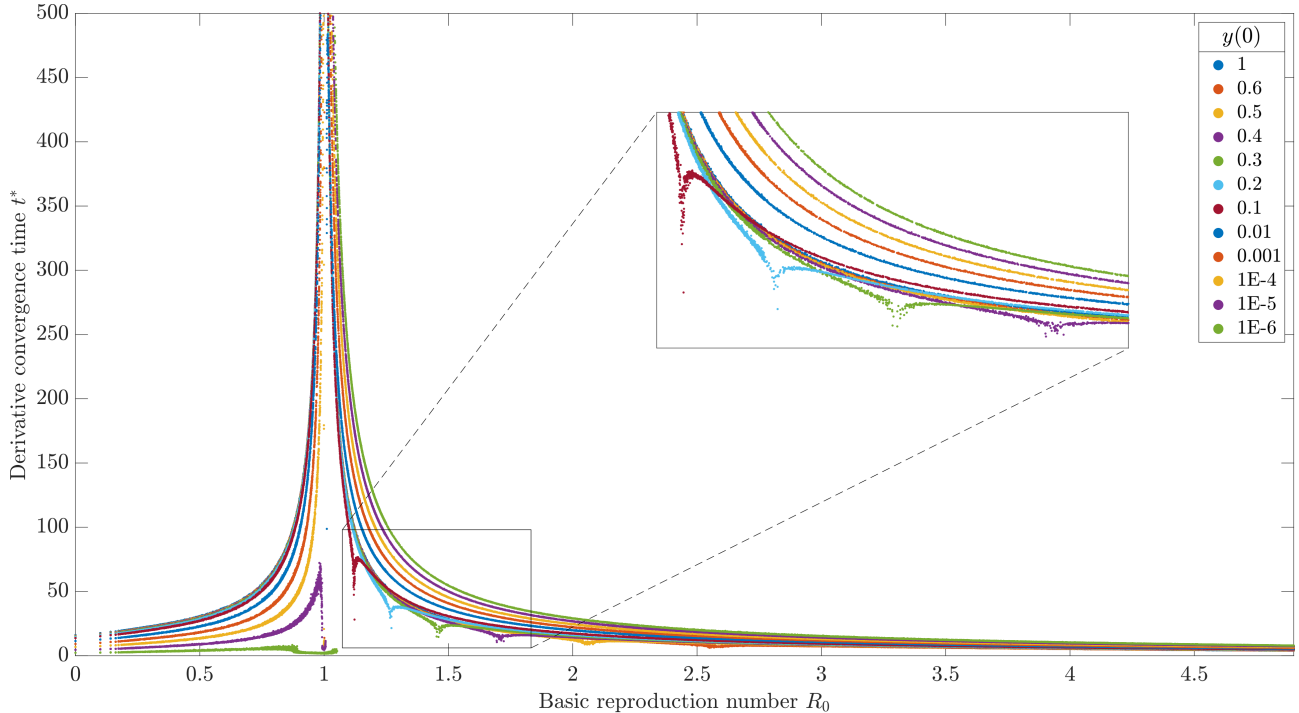


**Fig. 4** The derivative convergence time  $t^*$  versus the basic reproduction number  $R_0$  for different values of the starting prevalence  $y(0)$ . The chosen parameters are a graph size  $N = 50$ , accuracy tolerance  $r^* = 10^{-7}$ , infection rate  $\beta = 0.1$  and step-size  $h = 0.01$ . Each graph is a  $ER(N, p)$  graph with  $p \sim \text{Unif}(0, 1)$ . For  $R_0 > 1$ , the small values of  $y(0)$  are on top. For  $R_0 < 1$ , the small values of  $y(0)$  are at the bottom. The inset shows the dips below the curves in more detail.

**Theorem 1** (Theorem 5 in (Prasse et al., 2021)). *Consider two NIMFA systems with respective positive curing rates  $\delta_i$  and  $\tilde{\delta}_i$ , non-negative infection rates  $\beta_{ij}$  and  $\tilde{\beta}_{ij}$  and viral states  $v_i(t)$  and  $\tilde{v}_i(t)$ . Suppose that the initial viral states  $v_i(0)$  and  $\tilde{v}_i(0)$  are in  $[0, 1]$  for all nodes  $i$  and that matrices  $B$  and  $\tilde{B}$ , with elements  $\beta_{ij}$  and  $\tilde{\beta}_{ij}$ , respectively, are irreducible. Then, if  $\tilde{\delta}_i \leq \delta_i$  and  $\tilde{\beta}_{ij} \geq \beta_{ij}$  for all nodes  $i, j$ ,  $\tilde{V}(0) \geq V(0)$  implies that  $\tilde{V}(t) \geq V(t)$  at every time  $t$ .*

Additionally, Theorem 1 shows we do not have to consider mixed cases where  $v_i(0) > v_{\infty, i}$  for some  $i$ , but  $v_j(0) < v_{\infty, j}$  for some  $j \neq i$ , because then the decay of  $v_i(t)$  towards  $v_{\infty, i}$  will be faster than when  $v_j(0) \geq v_{\infty, j}$  and the growth of  $v_j(t)$  towards  $v_{\infty, j}$  will be faster than when  $v_i(0) \leq v_{\infty, i}$ . Indeed, in the decay situation, the  $\beta$  term in (3) is smaller when some nodes have to grow; vice-versa, for the growing case, the  $\beta$  term is bigger than the situation in which all nodes have to grow.

### 3.1 Upper bounds for the decay to the all healthy state and endemic steady state

The prevalence  $y(t; G, \tau, V(0))$  is the prevalence of the static NIMFA SIS process on the graph  $G$  with effective infection rate  $\tau$  and starting infection probability vector  $V(0)$ . For fixed effective infection rates  $\tau < \tau_c^{(1)}(K_N)$ , the slowest decay towards the all-healthy state  $V_\infty = 0$  occurs in the complete graph  $K_N$ . The decay is slowest on the complete graph, because each node  $i$  neighbours all other nodes  $j$ . Therefore, each node will receive the maximal possible infection attempts for each state vector  $V(t)$ . This is proven in Theorem 5 in (Prasse et al., 2021).

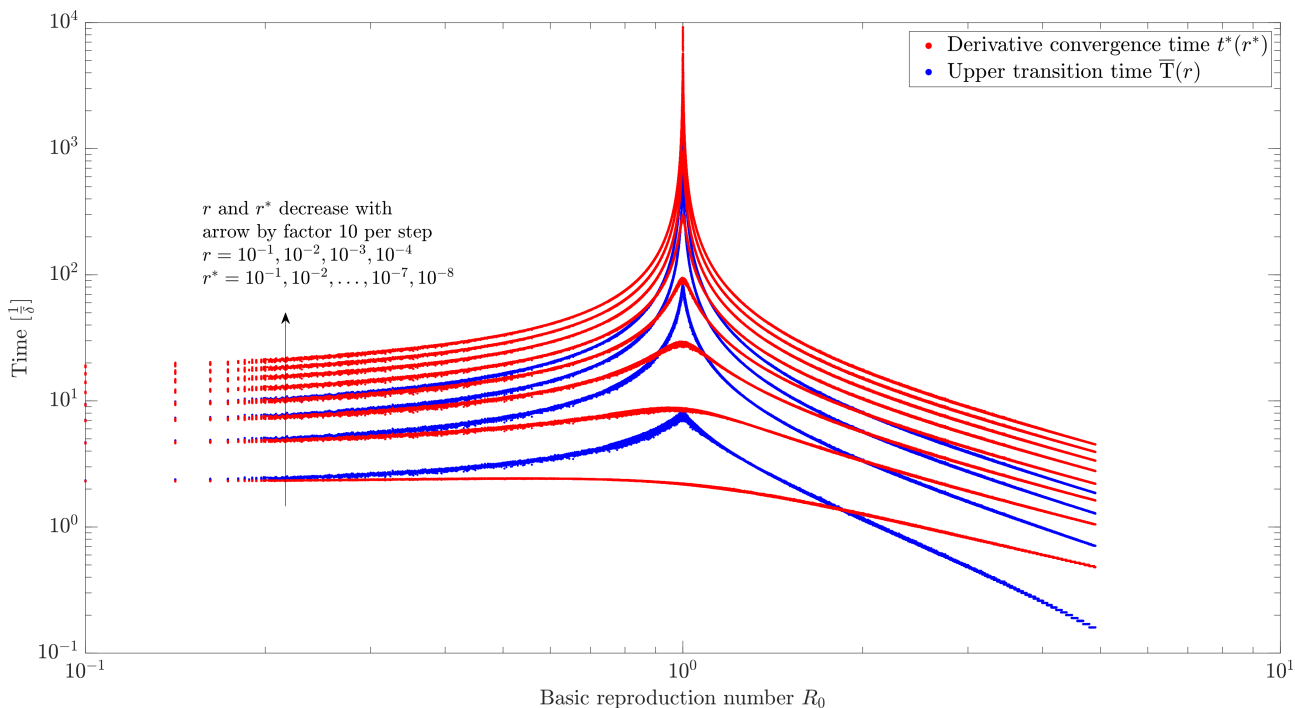


**Fig. 5** Comparison of the upper transition time  $\bar{T}(r)$  and the derivative convergence time  $t^*(r^*)$  for different values of  $r$  and  $r^*$ . The initial infection probability vector  $V(0) = u$  and time-step parameter  $h = 0.01$  are kept constant. The values of the accuracy tolerance  $r$  are  $10^{-1}, 10^{-2}, 10^{-3}, 10^{-4}$  and the values of the accuracy tolerance  $r^*$  are  $10^{-1}, 10^{-2}, \dots, 10^{-7}, 10^{-8}$ .

Based on extensive numerical simulations, we conjecture here that the prevalence  $y(t; K_N, \tau_c^{(1)}(K_N), u)$  on the complete graph  $K_N$  at the epidemic threshold  $\tau_c^{(1)}(K_N)$ , starting in the all-infected state  $V(0) = 1$ , decays slower than *any* prevalence  $y(t; G, \tau, u)$ , when  $\tau \leq \tau_c^{(1)}(G)$ , even if  $\tau_c^{(1)}(K_N) \leq \tau \leq \tau_c^{(1)}(G)$ . Additionally, we conjecture that the requirement  $\tau < \tau_c^{(1)}(G)$  is not necessary and that the prevalence  $y(t; K_N, \tau_c^{(1)}(K_N), u)$  also converges to the steady state  $V(0) = 0$  slower than any prevalence  $y(t; G, \tau, u)$  converges to its endemic steady state  $V_\infty(G)$  when  $\tau > \tau_c^{(1)}(G)$ . Some numerical results motivating both conjectures are given below (see Fig. 6). Additional substantiation for Conjecture 1 is provided in Appendix B.

First, we derive the prevalence  $y(t; K_N, \tau_c^{(1)}(K_N), u)$  by deriving the prevalence  $y(t; G, \tau_c^{(1)}(G), u)$  for any  $k$ -regular graph  $G$ .

**Lemma 2.** *For any  $k$ -regular graph  $G$ , the prevalence  $y(t; G, \tau_c^{(1)}(G), u)$  of the NIMFA SIS process on  $G$ , with effective infection rate  $\tau = \tau_c^{(1)}(G)$  with starting infection probability vector  $V(0) = u$  satisfies*

$$y(t; G, \tau_c^{(1)}(G), u) = \frac{1}{1+t}. \quad (11)$$

**Proof.** The graph  $G$  is  $k$ -regular and symmetry in (7) implies that  $v_i(t) = v_j(t) = y(t)$  for all nodes  $i$  and  $j$  when the starting infection probabilities  $v_i(0) = v_j(0)$  for all nodes  $i$  and  $j$ . We substitute  $v_i(t) = y(t)$  and the degree of each node  $d_i = \sum_{j=1}^N a_{ij} = k$  in (7) to obtain the following differential equation with initial condition  $y(0) = 1$ :

$$\frac{dy}{dt} = -y + \tau k(1-y)y.$$

For an effective infection rate  $\tau = \tau_c^{(1)}(G) = \frac{1}{k}$ , we find:

$$\frac{dy}{dt} = -y + (1 - y)y = -y^2. \quad (12)$$

The differential equation (12) has solution  $y(t) = \frac{1}{\frac{1}{y(0)} + t}$  and substituting  $y(0) = 1$  proves (11).  $\square$

**Conjecture 1.** *Given a graph  $G$  and  $\tau \leq \tau_c^{(1)}(G)$ , the prevalence  $y(t; G, \tau, V(0))$  of the epidemic process on  $G$  with effective infection rate  $\tau$  and starting infection probability vector  $V(0)$  satisfies*

$$y(t; G, \tau, V(0)) \leq y(t; G, \tau_c^{(1)}(G), u) \leq y(t; K_N, \tau_c^{(1)}(K_N), u) = \frac{1}{1+t}. \quad (13)$$

If Conjecture 1 is true, then the prevalence  $y(t) = \frac{1}{1+t}$  upper bounds the prevalence of all epidemic processes with  $R_0 \leq 1$ . In particular, it holds for disconnected graphs with  $R_0 \leq 1$ , since each subgraph corresponding to a connected component will have  $R_0 \leq 1$  and the prevalence of the disconnected graph is upper bounded by the largest subgraph prevalence.

Simulations in Fig. 6 agree with Conjecture 1 and suggest that the prevalence  $y(t; K_N, \tau_c^{(1)}(K_N), u)$  upper bounds not only decay processes with effective infection rate  $\tau \leq \tau_c^{(1)}$ , but converges slower to the steady-state prevalence  $y_\infty$  than any decay process, for any effective infection rate  $\tau$ . In Fig. 6, the green line represents  $y(t; K_N, \tau_c^{(1)}(K_N), u) = \frac{1}{1+t}$ . Each of the 100 blue lines per sub-figure corresponds to an ER-graph. In each figure,  $\tau$  is changed as a multiple of  $\tau_c^{(1)}(K_N)$  and the same for each graph. For the ER-graphs and several graphs with a fixed structure (including, for example, the path or star graph on  $N$  nodes), with arbitrary effective infection rate  $\tau$ , the decay from  $y(0) = 1$  to the steady-state prevalence  $y_\infty$  seems slower than for  $K_N$  with  $\tau = \tau_c^{(1)}(K_N)$ . Fig. 6 leads us to the second Conjecture:

**Conjecture 2.** *For any  $\tau > \tau_c$  the prevalence  $y(t; G, \tau, V(0))$  of the epidemic process on  $G$  with effective infection rate  $\tau$  starting in  $V(0) \geq V_\infty$  decays faster to  $V_\infty(G; \tau)$  than  $y(t; K_N, \tau_c^{(1)}(K_N), u)$  to  $V_\infty = 0$ . It holds that*

$$|y(t; G, \tau, V(0)) - y_\infty(G; \tau)| \leq |y(t; G, \tau, u) - y_\infty(G; \tau)| \leq y(t; K_N, \tau_c^{(1)}(K_N), u) = \frac{1}{1+t}.$$

If Conjecture 2 is true, it follows that  $y(t) = \frac{1}{1+t}$  upper bounds all decaying epidemic processes with  $R_0 > 1$  as well. Then, we can combine Conjecture 1 with Conjecture 2 and invert the upper bound to find that every static NIMFA process with  $V(0) \geq V_\infty$  will satisfy  $|y(t) - y_\infty| \leq r$  at time  $\frac{1-r}{r}$  such that

$$\bar{T}(r) \leq \frac{1-r}{r}. \quad (14)$$

For effective infection rates  $\tau \leq \tau_c^{(1)}$  we derive a second upper bound on  $\bar{T}(r)$  in Lemma 3, which diverges for  $R_0 \rightarrow 1$ , but which is tighter than (14) from  $R_0 = 0$  to the intersection point of both bounds, which will be derived after Lemma 3.

**Lemma 3.** *Given a graph  $G$  and  $\tau < \tau_c^{(1)}(G)$ , the prevalence  $y(t; G, \tau, V(0))$  of the epidemic process on  $G$  with effective infection rate  $\tau$  and starting infection probability vector  $V(0)$  satisfies*

$$y(t; G, \tau, V(0)) \leq y(t; G, \tau, u) \leq e^{(R_0(G, \tau) - 1)t}, \quad (15)$$

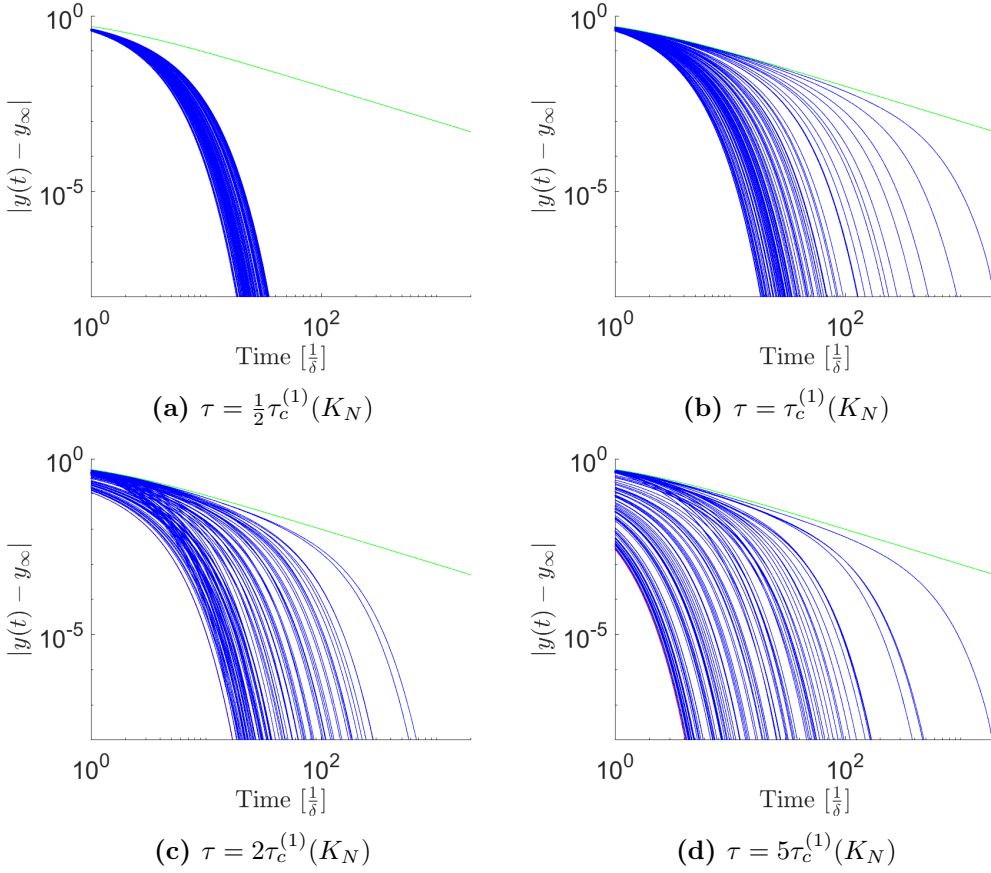


**Fig. 6** Error between the prevalence  $y(t)$  and the steady-state prevalence  $y_\infty$  (approximated by  $y(t_{\max})$ ) versus time. The green line is the function  $y(t) = \frac{1}{1+t}$ . Each of the blue curves is a different  $ER(N, p)$  graph where  $p \sim \text{Unif}(0, 1)$ . The effective infection rate  $\tau$  is varied for the different figures.

which leads to an upper bound on the upper transition time  $\bar{T}(r)$ :

$$\bar{T}(r) \leq \frac{1}{1 - R_0(G, \tau)} \log \left( \frac{1}{r} \right). \quad (16)$$

**Proof.** We start with the matrix NIMFA equation (6) and upper bound the derivative of the infection probability vector  $V(t)$  by disregarding the non-linear term. After rescaling time such that  $\delta = 1$  we find

$$\frac{dV(t)}{dt} \leq (\tau A - I)V(t), \quad (17)$$

whose solution is given in (Van Mieghem and Bovenkamp, 2013) as:

$$V(t) \leq e^{(\tau A - I)t} V(0). \quad (18)$$

After using the norm  $\|\cdot\|_2$  we obtain:

$$\|V(t)\|_2 \leq \|V(0)\|_2 e^{\lambda_1(\tau A - I)t} = \|V(0)\|_2 e^{(\tau \lambda_1(A) - 1)t} = \|V(0)\|_2 e^{(R_0(G, \tau) - 1)t}, \quad (19)$$

where the first inequality follows from:

$$\|e^M x\|_2 \leq \|e^M\|_2 \|x\|_2 \leq e^{\|M\|_2} \|x\|_2 = e^{\lambda_1(M)} \|x\|_2$$

where  $x$  is a  $N \times 1$  vector,  $M$  is a positive and symmetric  $N \times N$  matrix and  $\lambda_1(M)$  is the spectral radius of  $M$ .

Since  $\|V(t)\|_1 = Ny(t) \leq \sqrt{N}\|V(t)\|_2$ , we obtain from (19):

$$y(t) \leq \frac{\sqrt{N}}{N} \|V(t)\|_2 \leq \frac{1}{\sqrt{N}} \|V(0)\|_2 e^{(R_0(G,\tau)-1)t}. \quad (20)$$

Substituting  $\|V(0)\|_2 = \|u\|_2 = \sqrt{N}$  in (20) gives the right-hand side inequality in (15). Evaluating (15) at the time  $\mathcal{T} = \frac{1}{1-R_0(G,\tau)} \log\left(\frac{1}{r}\right)$  yields:

$$y(\mathcal{T}; G, \tau, V(0)) \leq e^{(R_0(G,\tau)-1)\frac{1}{1-R_0(G,\tau)} \log\left(\frac{1}{r}\right)} = e^{-\log\left(\frac{1}{r}\right)} = r, \quad (21)$$

from which the upper bound (16) follows.  $\square$

The upper bounds (14) and (16) complement each other, because the bound (14) is accurate around  $R_0 = 1$ , where the bound (16) diverges. We derive the value of the basic reproduction number  $R_0$  where the bounds intersect by solving  $\frac{1}{1-R_0} \log\left(\frac{1}{r}\right) = \frac{1-r}{r}$  for  $R_0$  and obtain

$$R_0 = 1 - \frac{r}{1-r} \log\left(\frac{1}{r}\right).$$

Since

$$\lim_{r \rightarrow 0} \frac{r}{1-r} \log\left(\frac{1}{r}\right) = 0,$$

the intersection is closer to  $R_0 = 1$  for stricter (smaller) accuracy tolerances  $r$ .

### 3.2 The upper bound for growth to the endemic steady state

For fixed  $\tau$  and graphs  $G$  with  $R_0(G, \tau) > 1$ , we briefly recall theory deduced in (Prasse and Van Mieghem, 2020).

**Assumption 1** (Assumption 1 in (Prasse and Van Mieghem, 2020)). *Assume that  $\delta_i > 0$  for all nodes  $i$  and  $\beta_{ij} \geq 0$  for all nodes  $i, j$ . Additionally, we assume in the limit of  $R_0 \downarrow 1$  that it holds that  $\delta_i \rightarrow 0$  and  $\delta_i \rightarrow \infty$  for all nodes  $i$ .*

Assumption 1 is trivially satisfied in our case, since we assume all  $\delta_i = \delta = 1$ , and all  $\beta_{ij} = \beta > 0$ .

**Assumption 2** (Assumption 3 in (Prasse and Van Mieghem, 2020)). *For every basic reproduction number  $R_0 > 1$ , the infection matrix  $B$  is symmetric and irreducible. Furthermore, in the limit  $R_0 \downarrow 1$ , the infection rate matrix  $B$  converges to a symmetric and irreducible matrix. This holds if and only if  $B$  (and its limit) corresponds to a connected undirected graph (Van Mieghem, 2014).*

Assumption 2 only considers connected graphs directly. If a graph has disconnected components, the analysis can be applied to the connected components separately, because the connected components are independent. Hence, it is natural to assume, without loss of generality, that the graph is connected.

**Lemma 4** (Corollary 1 in (Prasse and Van Mieghem, 2020)). *Suppose that Assumptions 1 and 2 hold and that the initial viral state  $V(0)$  equals  $V(0) = \xi_0 V_\infty$  for some scalar  $\xi_0 \in (0, 1)$ . Then, for any*

scalar  $\xi_1 \in [\xi_0, 1)$  the largest time  $\hat{t}$  at which the viral state satisfies  $V(\hat{t}) \leq \xi_1 v_{\infty, i}$  for every node  $i$  converges to

$$\hat{t} = \frac{\tau_c}{(\tau - \tau_c)\delta} \log \left( \frac{\xi_1 (1 - \xi_0)}{\xi_0 (1 - \xi_1)} \right), \quad (22)$$

when the basic reproduction number  $R_0$  approaches 1 from above.

**Lemma 5** (Equation 24 in (Prasse and Van Mieghem, 2020)). *Given Assumptions 1 and 2 and that the initial viral state  $V(0)$  is small or parallel to the steady-state vector  $V_\infty$  we have that*

$$\frac{v_i(t)}{v_j(t)} \rightarrow \frac{(x_1)_i}{(x_1)_j},$$

at every time  $t$  when  $R_0 \downarrow 1$ , where  $x_1$  is the non-negative eigenvector corresponding to the largest eigenvalue of the adjacency matrix  $A$ .

We will use Lemma 4 and Lemma 5 to upper bound the growth towards the steady state  $V_\infty(G)$  in Lemma 6. Lemma 4 gives an expression for the convergence time to the steady state  $\hat{t}$  up to a proportionality tolerance in the limit  $R_0 \downarrow 1$ . Lemma 5 ensures that we can pick the proportionality tolerance in such a way that the convergence time  $\hat{t}$  implies  $y(\hat{t}) \geq y_\infty - r$  in the limit  $R_0 \downarrow 1$ . The convergence time to the steady state  $\hat{t}$  is then an upper bound for the upper transition time  $\bar{T}(r)$  in the limit  $R_0 \downarrow 1$ . We derive this bound because the upper transition time  $\bar{T}(r)$  is largest for graphs around  $R_0 = 1$ . However, as shown in Section 3.5, the bound holds for all  $R_0 > 1$  in our numerical simulations. This is either because the error in  $\hat{t}$  is negative for large  $R_0$  (making (22) an upper bound for all  $R_0 > 1$ ) or because the additional bounding steps in the derivation are large enough for the bound to hold for bigger  $R_0$ . In the following we assume, without loss of generality, that the nodes  $i$  are labeled such that  $v_{\infty, 1} \geq v_{\infty, 2} \geq \dots \geq v_{\infty, N}$  and write  $d_{\max}$  for the highest degree in the graph  $G$ .

**Lemma 6** (Upper bound on  $\bar{T}(r)$  for growth). *For a connected graph  $G$ , it holds that for all  $V(0)$  with  $v_i(0) \in [r, v_{\infty, i}]$ , assuming  $|y(0) - y_\infty| > r$ , the upper transition time  $\bar{T}(r)$ ; the first time such that  $|y(\bar{T}(r)) - y_\infty| \leq r$ , is bounded by*

$$\bar{T}(r) \leq \frac{1}{R_0(G, \tau) - 1} \log \left( \frac{(1 - \frac{r}{v_{\infty, 1}})^2}{(\frac{r}{v_{\infty, 1}})^2} \right) \leq \frac{2}{R_0(G, \tau) - 1} \log \left( \frac{(r(\tau d_{\max} - 1) - \tau d_{\max})}{r(\tau d_{\max} - 1)} \right), \quad (23)$$

when the basic reproduction number  $R_0$  approaches 1 from above. When  $|y(0) - y_\infty| \leq r$ , the upper transition time  $\bar{T}(r) = 0$ .

**Proof.** By Theorem 1 we only need to bound the case when  $V(0) = ru$ . We consider Lemma 4 and take  $\xi_0 = \frac{r}{v_{\infty, 1}}$  and  $\xi_1 = (1 - \frac{r}{v_{\infty, 1}})$ . For all nodes  $i$ , it holds that  $\frac{v_{\infty, i}}{v_{\infty, 1}} \leq 1$ . We obtain:

$$v_i(0) = \xi_0 v_{\infty, i} = r \frac{v_{\infty, i}}{v_{\infty, 1}} \leq r,$$

$$\xi_1 v_{\infty, i} = \left(1 - \frac{r}{v_{\infty, 1}}\right) v_{\infty, i} = v_{\infty, i} - r \frac{v_{\infty, i}}{v_{\infty, 1}} \geq v_{\infty, i} - r.$$

With our chosen  $\xi_0$  and  $\xi_1$ , the requirements  $\xi_0 \in (0, 1)$  and  $\xi_1 \in [\xi_0, 1)$  in Lemma 4 become  $\frac{r}{v_{\infty, 1}} < 1$  and  $\frac{r}{v_{\infty, 1}} \leq 1 - \frac{r}{v_{\infty, 1}}$ , since  $\frac{r}{v_{\infty, 1}} > 0$  always holds.

When either inequality does not hold, we argue that  $|y(0) - y_\infty| < r$  and thus  $\bar{T}(r) = 0$ .

If  $\frac{r}{v_{\infty,1}} \geq 1$ , then we have  $v_{\infty,1} \leq r$  and thus  $|y(0) - y_{\infty}| \leq |r - v_{\infty,1}| < r$ . Similarly, if  $\frac{r}{v_{\infty,1}} > 1 - \frac{r}{v_{\infty,1}}$ , then  $\frac{r}{v_{\infty,1}} > \frac{v_{\infty,1} - r}{v_{\infty,1}}$ , implying that  $r > v_{\infty,1} - r$  and thus  $|y(0) - y_{\infty}| \leq |r - v_{\infty,1}| < r$ .

In both cases the upper transition time  $\bar{T}(r)$  is zero, since the starting prevalence  $y(0)$  is already closer to the steady-state prevalence  $y_{\infty}$  than the accuracy tolerance  $r$ .

With the choice of  $\xi_0 = \frac{r}{v_{\infty,1}}$  and  $\xi_1 = (1 - \frac{r}{v_{\infty,1}})$  the time  $\hat{t}$  in (22) is an upper bound for  $\bar{T}(r)$  in case of growth. Firstly, we have  $v_i(0) \leq r$  for all  $i$ , which lower bounds the allowed starting conditions  $v_i(0) \geq r$  from the definition (9). Then, Theorem 1 states that the growth from  $\xi_0 V_{\infty}$  is slower than the slowest growth considered for the upper transition time  $\bar{T}(r)$ , namely the growth from  $V(0) = ru$ . Secondly, in the limit  $R_0 \downarrow 1$ , at time  $\hat{t}$ , we have  $|v_i(\hat{t}) - v_{\infty,i}| \leq r$  for all nodes  $i$ . Lemma 4 states that  $|v_i(\hat{t}) - v_{\infty,i}| \leq r$  holds for at least one node  $i$ , but Lemma 5 guarantees that, for all nodes  $i$ , the value of  $\xi_1 v_{\infty,i}$  is reached at the same time  $\hat{t}$ , since the initial viral state vector  $V(0)$  is parallel to the steady-state vector  $V_{\infty}$ . After substituting  $\xi_0$  and  $\xi_1$  into Lemma 4, we find for  $V(0) < V_{\infty}$  on connected graphs that

$$\bar{T}(r) \leq \hat{t} = \frac{1}{R_0(G, \tau) - 1} \log \left( \frac{(1 - \frac{r}{v_{\infty,1}})^2}{(\frac{r}{v_{\infty,1}})^2} \right), \quad (24)$$

where we have replaced  $\frac{\tau_c}{(\tau - \tau_c)\delta}$  in (22) with  $\frac{1}{R_0(G, \tau) - 1}$ , because we take  $\delta = 1$  and

$$\frac{\tau_c^{(1)}(G)}{\tau - \tau_c^{(1)}(G)} = \frac{\frac{\tau}{R_0(G, \tau)}}{\tau - \frac{\tau}{R_0(G, \tau)}} = \frac{\tau}{R_0(G, \tau)\tau - \tau} = \frac{1}{R_0(G, \tau) - 1}.$$

Finally, we can upper bound  $v_{\infty,1}$  invoking equation (15) from (Van Mieghem et al., 2009):

$$0 \leq v_{\infty,i} \leq 1 - \frac{1}{1 + \tau d_i}, \quad (25)$$

where  $d_i$  is the degree of node  $i$ . Equation (25) implies that  $v_{\infty,i} \leq 1 - \frac{1}{1 + \tau d_{\max}}$  for all nodes  $i$  and thus  $v_{\infty,1} \leq 1 - \frac{1}{1 + \tau d_{\max}}$ . Substituting this upper bound into (24) and taking the squares out of the logarithm proves the second inequality in (23).  $\square$

### 3.3 Summary: the general upper bound for time-variant networks

We have conjectured and proved upper bounds for individual graphs on  $\bar{T}(r)$  for decay processes in (14) and (16) and proved an upper bound for growth on connected graphs in Lemma 6. We combine the results and define an upper bound  $\hat{T}_c(r, G)$  on  $\bar{T}(r)$  for a connected graph:

$$\hat{T}_c(r, G) = \begin{cases} \frac{1}{1 - R_0(G, \tau)} \log \left( \frac{1}{r} \right) & \text{if } R_0(G, \tau) \leq 1 - \frac{r}{1 - r} \log \left( \frac{1}{r} \right), \\ \frac{1 - r}{r} & \text{if } 1 - \frac{r}{1 - r} \log \left( \frac{1}{r} \right) \leq R_0(G, \tau) \leq 1, \\ \max \left( \frac{1 - r}{r}, \left( \frac{2}{R_0(G, \tau) - 1} \log \left( \frac{(r(\tau d_{\max}(G) - 1) - \tau d_{\max}(G))^2}{r^2 (\tau d_{\max}(G) - 1)^2} \right) \right) \right) & \text{if } R_0(G, \tau) > 1. \end{cases} \quad (26)$$

For disconnected simple graphs, the process on each of the components is completely independent. We can upper bound the convergence of the components separately using (26). Consider a general

graph  $G$  with connected component subgraphs  $C_1, \dots, C_K$ , we define the upper bound  $\hat{T}(r, G)$ :

$$\hat{T}(r, G) = \max_{C_k} \left\{ \hat{T}_c(r, C_k) \right\}. \quad (27)$$

Since definition (27) also holds for connected graphs, we write our general upper bound for  $\bar{T}(r)$  for a set or sequence of graphs  $\mathcal{G}$  as

$$\bar{T}(r, \mathcal{G}) \leq \max_{G \in \mathcal{G}} \left\{ \hat{T}(r, G) \right\} = \max_{G \in \mathcal{G}} \left\{ \max_{C_k} \left\{ \hat{T}_c(r, C_k) \right\} \right\}. \quad (28)$$

### 3.4 Lower bounds for the upper transition time

Inequality (20) allows us to find a non-trivial lower bound for  $\bar{T}(r)$  in growth processes.

**Lemma 7.** *Given a graph  $G$ , an effective infection rate  $\tau > \tau_c^{(1)}(G)$  and an accuracy tolerance  $r$ , the upper transition time  $\bar{T}(r)$  has a lower bound for growth given by*

$$\bar{T}(r) \geq \frac{1}{(R_0(G, \tau) - 1)} \log \left( \frac{y_\infty(G) - r}{r} \right). \quad (29)$$

**Proof.** The slowest growth starts in the lowest allowed starting probability vector  $V(0) = ru$  (recall Theorem 1). We have  $\|V(0)\|_2 = \|ru\|_2 = \sqrt{Nr}$ . Substituting in (20) gives

$$y(t) \leq r e^{(R_0(G, \tau) - 1)t}$$

where  $R_0(G, \tau) - 1$  is now positive, contrary to Lemma 3. The time  $\mathcal{T}$  such that

$$r e^{(R_0(G, \tau) - 1)\mathcal{T}} = y_\infty(G) - r \quad (30)$$

bounds  $\bar{T}(r)$  from below, because  $y(\mathcal{T}) \leq r e^{(R_0(G, \tau) - 1)\mathcal{T}} = y_\infty(G) - r$ . We solve (30) for  $\mathcal{T}$  and find (29).  $\square$

We also determine the following lower bound for decay processes.

**Lemma 8.** *Given a graph  $G$ , an effective infection rate  $\tau$  and an accuracy tolerance  $r$ , the upper transition time  $\bar{T}(r)$  has a lower bound for decay given by*

$$\bar{T}(r) \geq \log \left( \frac{1}{y_\infty(G) + r} \right). \quad (31)$$

**Proof.** We consider a decay process and lower bound its prevalence by ignoring the infection process. We have at all times  $t$  that  $\frac{dy}{dt} \geq -y$ , by ignoring the second term in (7) and summing over the infection probabilities  $v_i$ . Using Grönwall's Lemma we obtain  $y(t) \geq y(0)e^{-t}$ . The highest lower bound occurs when  $y(0) = 1$  (recall Theorem 1) and we obtain  $|y(t) - y_\infty(G)| \geq e^{-t} - y_\infty(G)$ . We find that  $t = \mathcal{T} = \log \left( \frac{1}{y_\infty(G) + r} \right)$  is the time such that  $e^{-t} = y_\infty(G) + r$  and therefore a lower bound on  $\bar{T}(r)$  in a decay process, because  $|y(\mathcal{T}) - y_\infty| \geq e^{-\mathcal{T}} - y_\infty(G) = r$ .  $\square$

### 3.5 Evaluation of the bounds

We simulate the upper transition time  $\bar{T}(r)$ , with  $r = 10^{-4}$  for the extreme values of  $V(0)$ , namely,  $V(0) = u$  and  $V(0) = ru$ . Fig. 7 shows the upper transition time  $\bar{T}(r)$  together with the bounds from Section 3. The upper bound on decay (16) is remarkably accurate for  $R_0 \leq 1$ , but the upper bound (14) is less sharp for  $R_0 > 1$ . This is expected, because the upper bound (14) is an upperbound of the asymptote at  $R_0 = 1$ . The upper bound on growth (23) is a solid bound for the upper transition time  $\bar{T}(r)$  for growth. The lower bound on growth (29) unexpectedly fits the upper transition time  $\bar{T}(r)$  for decay very well for  $R_0 > 1$ . The lower bound on decay (31) is weak. Although not clearly visible, all bounds hold for all  $R_0$ . The upper bound on decay (16) and the lower bound on growth (29) are both derived from the same approximation (20), but (29) seems to perform worse than (16).

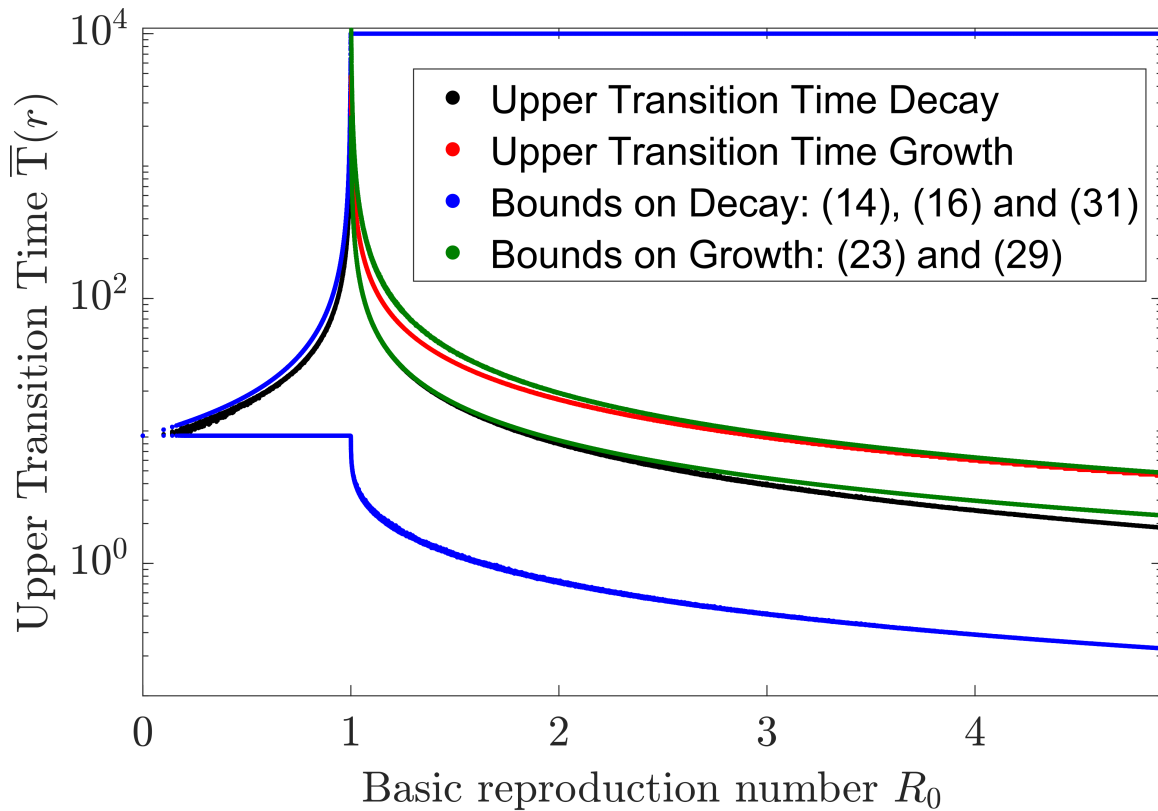


**Fig. 7** Comparison of the analytically derived bounds and numerically determined upper transition time  $\bar{T}(r)$ , with  $r = 10^{-4}$ . The upper transition time  $\bar{T}(r)$  is shown for  $y(0) = 1$  in black as bound for decay and for  $y(0) = r$  in red as bound for growth. The blue lines are the bounds on decay (black) and the green lines are the bounds on growth (red).

## 4 Conclusions

The interplay of the topological process and the epidemic process is a substantial challenge in the analysis of general epidemics on time-variant networks. Timescale separation often restricts studies to simpler scenarios, where the network is assumed static or approximated by the average of time-variant networks. However, in real-world epidemics the network does change at a comparable speed compared

to the epidemic process. Hence, a thorough understanding of the intermediate regime, where the timescales cannot be separated, is vital for a realistic and reliable modelling approach.

In this work, a first step towards the analysis of the intermediate regime is presented. We define the upper transition time  $\bar{T}(r)$ , a threshold quantity which characterizes the border of the intermediate regime and the *quenched* regime, in which the network is qualitatively static. This threshold quantity  $\bar{T}(r)$  can be used in an analysis of an SIS epidemic to determine whether a network can be assumed to be static. Indeed, when the inter-update time  $\Delta t$  is larger than  $\bar{T}(r)$ , the epidemic process can, in most situations, be accurately predicted. We show that for fixed parameters, but different graphs, the basic reproduction number  $R_0$  determines the upper transition time  $\bar{T}(r)$ . We derive upper and lower bounds for the upper transition time  $\bar{T}(r)$  in (28), (29) and (31), and compare them in Fig. 7 to numerical estimations of  $\bar{T}(r)$ . We introduce the derivative convergence time  $t^*(r^*)$ , to upper bound the upper transition time  $\bar{T}(r)$  and we argue that  $t^*(r^*)$  is easier to determine numerically, although the time saved varies depending on how one determines the steady-state prevalence  $y_\infty$ . Additionally, we show that the upper transition time  $\bar{T}(r)$  is large when networks around the epidemic threshold are present in the temporal process. Some real-world epidemics, e.g. influenza, are characterized by  $R_0$  slightly above the epidemic threshold (Biggerstaff et al., 2014). For similar diseases around the epidemic threshold, our work shows that the upper transition time  $\bar{T}(r)$  is large in units of  $\frac{1}{\delta}$ . This implies that these real-world epidemics are in the intermediate regime; hence, we expect that the network topology updates play an active role in the disease spread. Additionally, the limits on the predictability of the process even if  $\Delta t \geq \bar{T}(r)$ , as explained in Section 2, show that even in the approximate quenched regime, temporal effects are not negligible in general.

We leave various open paths for future work, among which: 1) investigating a heterogeneous NIMFA SIS; 2) considering inter-update times  $T_m$  that are random variables with arbitrary distributions  $F_{T_m}(x) = \Pr[T_m \leq x]$  instead of fixed  $\Delta t$  as here; and 3) considering a Markovian time-variant SIS process besides NIMFA.

Since the lower transition time  $\underline{T}(r)$  is not as easily defined as the upper transition time, an analysis of the lower boundary of the intermediate regime is also a promising topic for further analysis.

Lastly, while our bounds (28), (29) and (31) are general, our simulations of  $\bar{T}(r)$  were limited to ER-graphs only. We show in Appendix A that different networks do not behave significantly different for  $N = 50$ . However, a thorough verification of our results on different classes of networks would certainly be of interest.

## A Assumption of ER-graphs

Fig. 8 illustrates that for  $N = 50$  the ER-graphs are representative of general graphs. For each graph type (Barabasi-Albert (BA), Erdős-Rényi (ER) and Watts-Strogatz (WS)) the upper transition time  $\bar{T}(r)$  is plotted. Each of the 9000 graphs have, except for  $N$ , uniformly distributed parameters<sup>5</sup>. ER-graphs have one parameter: the link density  $p \sim \text{Unif}[0, 1]$ . BA-graphs have two parameters: the size of the starting clique  $m_0 \sim \text{Unif}\{1, N\}$  and the degree of nodes when attached  $m \sim \text{Unif}\{1, m_0\}$ .

<sup>5</sup>We denote  $\text{Unif}(a, b)$  for the continuous uniform distribution on the interval  $[a, b]$  and  $\text{Unif}\{a, b\}$  for the discrete uniform distribution on the set  $\{a, a + 1, \dots, b - 1, b\}$

WS-graphs have two parameters: the average degree divided by two  $K \sim \text{Unif}\{1, \lfloor \frac{N-1}{2} \rfloor\}$  and the rewiring probability  $\beta_{WS} \sim \text{Unif}[0, 1]$ . The differences between the three types of graphs are negligible but not nonexistent. It is plausible that these differences will become larger when  $N$  increases. Fig. 9, which is the same as Fig. 8 but with logarithmic axes, illustrates that, while the absolute differences are negligible, there is already a significant relative difference between ER/WS and BA graphs.

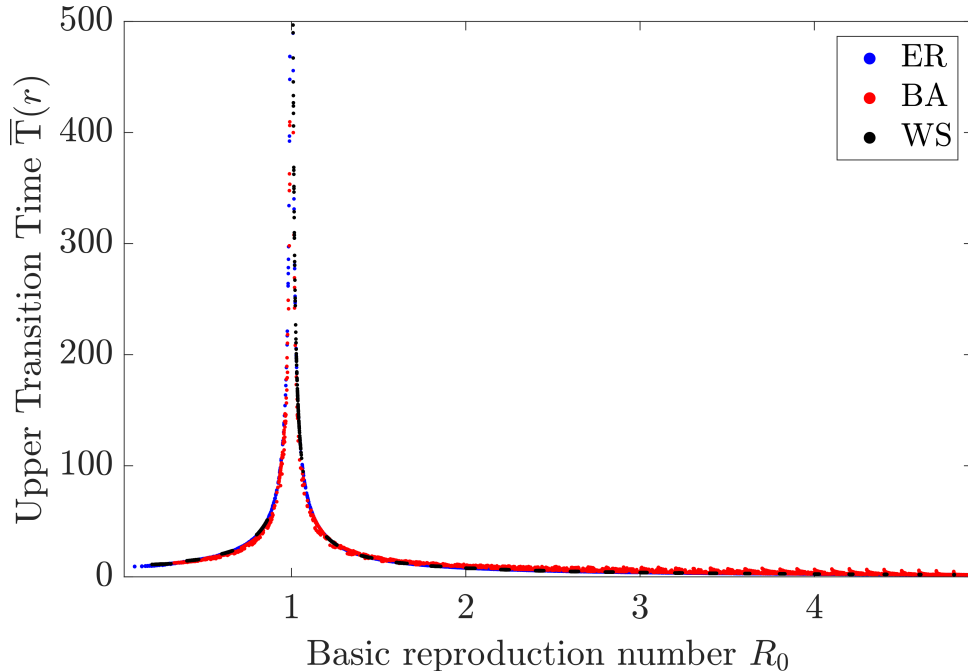


**Fig. 8** The upper transition time  $\bar{T}(r)$  versus basic reproduction number  $R_0$  for three different graph types. Shown is the decay process starting in  $V(0) = u$ , for  $N = 50$  and  $\beta = 0.1$ . In blue, 3000 Erdős-Rényi graphs with uniformly distributed parameters ( $G_p(N)$  with  $p \sim \text{Unif}(0, 1)$ ). In red, 3000 Barabasi-Albert graphs with uniformly distributed parameters ( $m_0 \sim \text{Unif}\{1, N\}$  and  $m \sim \text{Unif}\{1, m_0\}$ ). In black, 3000 Watts-Strogatz graphs with uniformly distributed parameters ( $K \sim \text{Unif}\{1, \lfloor \frac{N-1}{2} \rfloor\}$  and  $\beta_{WS} \sim \text{Unif}(0, 1)$ ).

## B Substantiation for Conjecture 1

In this section, we present a proof outline for Conjecture 1, highlighting which steps are missing. We restrict ourselves to the case of  $\tau = \tau_c^{(1)}(G)$  since that case is an upper bound for other  $\tau < \tau_c^{(1)}(G)$ . We denote the projection of the viral state vector  $V(t)$  on the principal eigenvector  $x_1$  of the adjacency matrix  $A$  as

$$c(t) = x_1^T V(t). \quad (32)$$

Then, the viral state vector  $V(t)$  can be written as a linear combination of two vectors

$$V(t) = c(t)x_1(t) + \xi(t), \quad (33)$$

where the  $N \times 1$  vector

$$\xi(t) = V(t) - c(t)x_1(t) \quad (34)$$

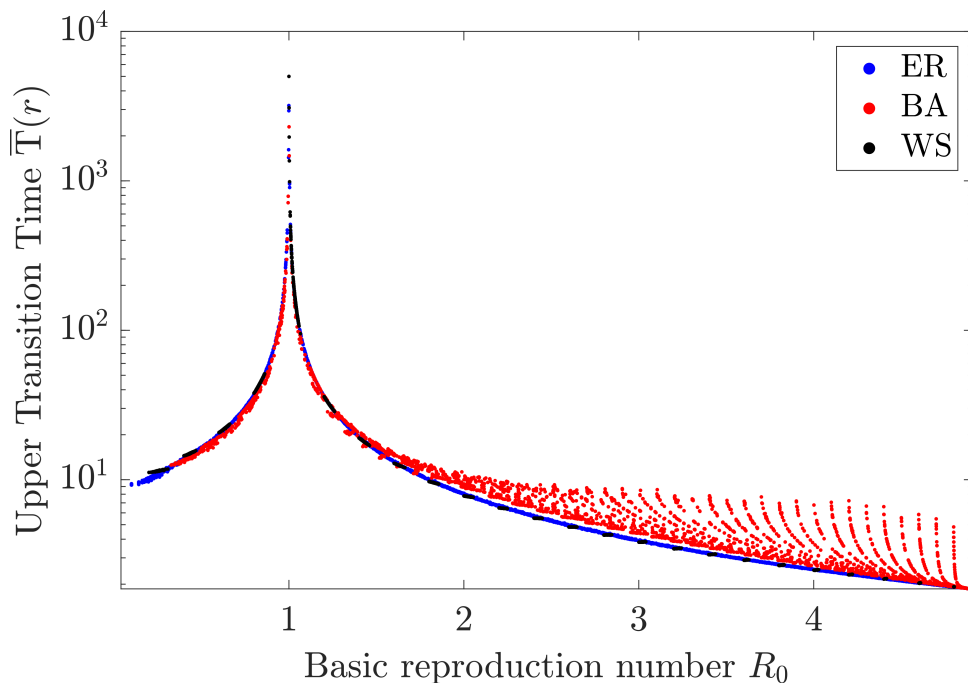


**Fig. 9** The upper transition time  $\bar{T}(r)$  versus basic reproduction number  $R_0$  for three different graph types. Shown is the decay process starting in  $V(0) = u$ , for  $N = 50$  and  $\beta = 0.1$ . In blue, 3000 Erdős-Rényi graphs with uniformly distributed parameters ( $G_p(N)$  with  $p \sim \text{Unif}(0, 1)$ ). In red, 3000 Barabasi-Albert graphs with uniformly distributed parameters ( $m_0 \sim \text{Unif}\{1, N\}$  and  $m \sim \text{Unif}\{1, m_0\}$ ). In black, 3000 Watts-Strogatz graphs with uniformly distributed parameters ( $K \sim \text{Unif}\{1, \lfloor \frac{N-1}{2} \rfloor\}$  and  $\beta_{WS} \sim \text{Unif}(0, 1)$ ).

is orthogonal to the principal eigenvector, i.e.,  $x_1^T \xi(t) = 0$ . At the initial time  $t = 0$ , using  $V(0) = u$  the decomposition of the viral state vector  $V(0)$  in (33) becomes

$$V(0) = c(0)x_1 + \xi(0) = u. \quad (35)$$

We rewrite the definition (1) of the prevalence  $y(t)$  as

$$y(t) = \frac{1}{N} u^T V(t),$$

which yields with (33) and (35) that

$$y(t) = \frac{1}{N} (c(0)x_1 + \xi(0))^T (c(t)x_1 + \xi(t)). \quad (36)$$

Since  $x_1^T \xi(t) = 0$  at every time  $t$  and  $x_1^T x_1 = 1$ , we obtain that

$$Ny(t) = c(0)c(t) + \xi(0)^T \xi(t). \quad (37)$$

To prove that  $y(t) \leq \frac{1}{1+t}$  is an upperbound of the prevalence  $y(t)$ , we apply the triangle inequality to (37), which implies that the prevalence  $y(t)$  of any graph obeys

$$Ny(t) \leq c(0)c(t) + |\xi(0)^T \xi(t)|,$$

at every time  $t$ . Here we used  $|c(0)c(t)| = c(0)c(t)$ , since (32) and  $v_i(t) \geq 0$  for every node  $i$  at every time  $t$  implies that  $c(t) \geq 0$  at every time  $t$ . Furthermore, we apply the Cauchy-Schwarz inequality to obtain that

$$Ny(t) \leq c(0)c(t) + \|\xi(0)\|_2 \|\xi(t)\|_2.$$

To prove Conjecture 1, it remains to show that

$$c(0)c(t) + \|\xi(0)\|_2 \|\xi(t)\|_2 \leq \frac{N}{1+t}, \quad (38)$$

at every time  $t$ . Numerical simulations suggest that this inequality holds. To further specify a proof direction we consider a regular graph. For a regular graph it holds that  $x_1 = \frac{1}{\sqrt{N}}u$  and  $\xi(t) = 0$  for all times  $t$ . Solving the NIMFA equations (7) we find that

$$c(t) = \frac{\sqrt{N}}{1+t}.$$

Hence, since  $c(0) = \sqrt{N}$  for a regular graph we obtain

$$c(t) \leq \frac{c(0)}{1+t}.$$

Now, if a graph is not a regular graph, then the eigenvector  $x_1$  is not a multiple of the all-one vector  $u$ , which implies that  $\|\xi(0)\|_2 > 0$ . Intuitively speaking, the less regular a graph is, the smaller  $c(t)$  and the larger  $\|\xi(t)\|_2$  should be. It is therefore reasonable to assume one could prove that

$$c(t) \leq c(0) \frac{1}{1+t}. \quad (39)$$

We have not been able to prove (39). However, like (38), numerical simulations suggest that the inequality holds. In Theorem 2 from (Prasse and Van Mieghem, 2020) a similar decomposition is used in which the error term  $\|\xi(t)\|_2$  was bounded by a formula of the shape

$$\|\xi(t)\|_2 \leq \|\xi(0)\|_2 e^{-\sigma t},$$

at all times  $t$  for some constant  $\sigma > 0$ . Now, suppose that one can show that the same inequality holds in this case and that  $\sigma = 1$ . Then, after using  $e^{-\sigma t} \leq e^{-t} \leq \frac{1}{1+t}$  we would find

$$\|\xi(t)\|_2 \leq \|\xi(0)\|_2 \frac{1}{1+t}, \quad (40)$$

which has also been numerically verified. After substituting (40) and (39) the left side of (38) becomes

$$c(0)c(t) + \|\xi(0)\|_2 \|\xi(t)\|_2 \leq c^2(0) \frac{1}{1+t} + \|\xi(0)\|_2^2 \frac{1}{1+t} = \|V(0)\|_2^2 \frac{1}{1+t} = \frac{\sqrt{N}}{1+t}, \quad (41)$$

where the terms can be combined due to the orthogonality of  $x_1$  and  $\xi(0)$  and the last equality follows from  $V(0) = u$ . Note that this would prove Conjecture 1 by showing (38). We emphasise that Equations (38), (39) and (40) have been numerically verified. Combined with the results shown in Fig. 6, we believe that there is strong numerical evidence for Conjecture 1.

## References

- R. M. Anderson and R. M. May. *Infectious diseases of humans: dynamics and control*. Oxford university press, 1991.
- M. Biggerstaff, S. Cauchemez, C. Reed, M. Gambhir, and L. Finelli. Estimates of the reproduction number for seasonal, pandemic, and zoonotic influenza: a systematic review of the literature. *BMC infectious diseases*, 14(1):1–20, 2014.
- E. Cator and P. Van Mieghem. Second-order mean-field susceptible-infected-susceptible epidemic threshold. *Physical review E*, 85(5):056111, 2012.
- K. Devriendt and P. Van Mieghem. Unified mean-field framework for susceptible-infected-susceptible epidemics on networks, based on graph partitioning and the isoperimetric inequality. *Physical Review E*, 96(5):052314, 2017.
- A. Ganesh, L. Massoulié, and D. Towsley. The effect of network topology on the spread of epidemics. In *Proceedings IEEE 24th Annual Joint Conference of the IEEE Computer and Communications Societies.*, volume 2, pages 1455–1466. IEEE, 2005.
- H. Guo, Q. Yin, C. Xia, and M. Dehmer. Impact of information diffusion on epidemic spreading in partially mapping two-layered time-varying networks. *Nonlinear Dynamics*, 105(4):3819–3833, 2021.
- L. Han, Z. Lin, M. Tang, Y. Liu, and S. Guan. Impact of human contact patterns on epidemic spreading in time-varying networks. *Physical Review E*, 107(2):024312, 2023.
- P. Holme. Modern temporal network theory: a colloquium. *The European Physical Journal B*, 88:1–30, 2015.
- P. Holme and F. Liljeros. Birth and death of links control disease spreading in empirical contact networks. *Scientific reports*, 4(1):4999, 2014.
- P. Holme and J. Saramäki. Temporal networks. *Physics reports*, 519(3):97–125, 2012.
- A. Khanafer, T. Başar, and B. Gharesifard. Stability of epidemic models over directed graphs: A positive systems approach. *Automatica*, 74:126–134, 2016.
- V. Kohar and S. Sinha. Emergence of epidemics in rapidly varying networks. *Chaos, Solitons & Fractals*, 54:127–134, 2013.
- B. Kotnis and J. Kuri. Stochastic analysis of epidemics on adaptive time varying networks. *Physical Review E*, 87(6):062810, 2013.
- A. Lajmanovich and J. A. Yorke. A deterministic model for gonorrhoea in a nonhomogeneous population. *Mathematical Biosciences*, 28(3-4):221–236, 1976.
- J. Leitch, K. A. Alexander, and S. Sengupta. Toward epidemic thresholds on temporal networks: a review and open questions. *Applied Network Science*, 4:1–21, 2019.
- C. Li, R. van de Bovenkamp, and P. Van Mieghem. Susceptible-infected-susceptible model: A comparison of N-intertwined and heterogeneous mean-field approximations. *Physical Review E*, 86(2):026116, 2012.
- E. Lieberman, C. Hauert, and M. A. Nowak. Evolutionary dynamics on graphs. *Nature*, 433(7023):312–316, 2005.
- W. Mei, S. Mohagheghi, S. Zampieri, and F. Bullo. On the dynamics of deterministic epidemic propagation over networks. *Annual Reviews in Control*, 44:116–128, 2017.
- M. Nadini, K. Sun, E. Ubaldi, M. Starnini, A. Rizzo, and N. Perra. Epidemic spreading in modular time-varying networks. *Scientific reports*, 8(1):2352, 2018.
- C. Nowzari, V. M. Preciado, and G. J. Pappas. Analysis and control of epidemics: A survey of spreading processes on complex networks. *IEEE Control Systems Magazine*, 36(1):26–46, 2016.

- M. Ogura and V. M. Preciado. Stability of spreading processes over time-varying large-scale networks. *IEEE Transactions on Network Science and Engineering*, 3(1):44–57, 2016.
- P. E. Paré, C. L. Beck, and A. Nedić. Stability analysis and control of virus spread over time-varying networks. In *2015 54th IEEE Conference on Decision and Control (CDC)*, pages 3554–3559. IEEE, 2015.
- P. E. Paré, C. L. Beck, and A. Nedić. Epidemic processes over time-varying networks. *IEEE Transactions on Control of Network Systems*, 5(3):1322–1334, 2017a.
- P. E. Paré, J. Liu, C. L. Beck, A. Nedić, and T. Başar. Multi-competitive viruses over static and time-varying networks. In *2017 American Control Conference (ACC)*, pages 1685–1690. IEEE, 2017b.
- R. Pastor-Satorras and A. Vespignani. Epidemic spreading in scale-free networks. *Physical review letters*, 86(14):3200, 2001a.
- R. Pastor-Satorras and A. Vespignani. Epidemic dynamics and endemic states in complex networks. *Physical Review E*, 63(6):066117, 2001b.
- R. Pastor-Satorras, C. Castellano, P. Van Mieghem, and A. Vespignani. Epidemic processes in complex networks. *Reviews of modern physics*, 87(3):925–979, 2015.
- N. Perra, B. Gonçalves, R. Pastor-Satorras, and A. Vespignani. Activity driven modeling of time varying networks. *Scientific reports*, 2(1):469, 2012.
- B. A. Prakash, H. Tong, N. Valler, M. Faloutsos, and C. Faloutsos. Virus propagation on time-varying networks: Theory and immunization algorithms. In *Machine Learning and Knowledge Discovery in Databases: European Conference, ECML PKDD 2010, Barcelona, Spain, September 20-24, 2010, Proceedings, Part III 21*, pages 99–114. Springer, 2010.
- B. Prasse and P. Van Mieghem. Time-dependent solution of the NIMFA equations around the epidemic threshold. *Journal of mathematical biology*, 81(6):1299–1355, 2020.
- B. Prasse, K. Devriendt, and P. Van Mieghem. Clustering for epidemics on networks: A geometric approach. *Chaos: an interdisciplinary journal of nonlinear science*, 31(6):063115, 2021.
- G. Ren and X. Wang. Epidemic spreading in time-varying community networks. *Chaos: An Interdisciplinary Journal of Nonlinear Science*, 24(2):023116, 2014.
- Y. Schwarzkopf, A. Rákos, and D. Mukamel. Epidemic spreading in evolving networks. *Physical Review E*, 82(3):036112, 2010.
- J. Stehlé, N. Voirin, A. Barrat, C. Cattuto, V. Colizza, L. Isella, C. Régis, J.-F. Pinton, N. Khanafer, W. Van den Broeck, et al. Simulation of an SEIR infectious disease model on the dynamic contact network of conference attendees. *BMC medicine*, 9(1):1–15, 2011.
- E. Valdano, M. R. Fiorentin, C. Poletto, and V. Colizza. Epidemic threshold in continuous-time evolving networks. *Physical review letters*, 120(6):068302, 2018.
- P. Van Mieghem. *Graph spectra for complex networks*. Cambridge University Press, Cambridge, U.K., 2011a.
- P. Van Mieghem. The N-intertwined SIS epidemic network model. *Computing*, 93(2):147–169, 2011b.
- P. Van Mieghem. Decay towards the overall-healthy state in SIS epidemics on networks. *arXiv preprint arXiv:1310.3980*, 2013.
- P. Van Mieghem. *Performance analysis of complex networks and systems*. Cambridge University Press, 2014.
- P. Van Mieghem. Explosive phase transition in susceptible-infected-susceptible epidemics with arbitrary small but nonzero self-infection rate. *Physical Review E*, 101(3):032303, 2020.

- P. Van Mieghem and R. van de Bovenkamp. Non-Markovian infection spread dramatically alters the susceptible-infected-susceptible epidemic threshold in networks. *Physical review letters*, 110(10):108701, 2013.
- P. Van Mieghem, J. Omic, and R. Kooij. Virus spread in networks. *IEEE/ACM Transactions On Networking*, 17(1):1–14, February 2009.
- C. L. Vestergaard and M. Génois. Temporal Gillespie algorithm: fast simulation of contagion processes on time-varying networks. *PLoS computational biology*, 11(10):e1004579, 2015.
- Y.-Q. Zhang, X. Li, and A. V. Vasilakos. Spectral analysis of epidemic thresholds of temporal networks. *IEEE transactions on cybernetics*, 50(5):1965–1977, 2017.